

Validation and calibration of a high-cycle accumulation model based on cyclic triaxial tests on eight sands

T. Wichtmannⁱ⁾ A. Niemunisⁱⁱ⁾ Th. Triantafyllidisⁱⁱⁱ⁾

Abstract: The high-cycle accumulation (HCA) model proposed by Niemunis et al. [25] predicts permanent deformations in non-cohesive soils due to many cycles ($N > 10^3$) with relatively small amplitudes ($\varepsilon^{\text{ampl}} < 10^{-3}$, so-called high- or polycyclic loading). This paper demonstrates the applicability of the HCA model to different sands. For this purpose, approximately 200 triaxial tests with 10^5 cycles each have been performed on eight different quartz sands with mean grain sizes in the range $0.15 \text{ mm} \leq d_{50} \leq 4.4 \text{ mm}$ and coefficients of uniformity in the range $1.3 \leq U_c \leq 4.5$. For each sand, test series with a variation of stress amplitude, initial relative density, average mean pressure p^{av} and average stress ratio $\eta^{\text{av}} = q^{\text{av}}/p^{\text{av}}$ have been conducted. The influence of the grain size distribution curve on the rate of strain accumulation is discussed. A comparison of the measured data with predictions made by the HCA model (with different material constants) is given. Correlations of the material constants with index or granulometric properties are discussed. The correlations may be useful for a simplified procedure to determine a set of material constants.

Keywords: sand, high-cyclic loading, accumulation of strain, high-cycle accumulation model, cyclic triaxial tests, grain size distribution curve

1 Introduction

The present paper deals with the accumulation of residual strain in non-cohesive soils subjected to a drained cyclic loading with many cycles ($N > 10^3$) and relatively small strain amplitudes ($\varepsilon^{\text{ampl}} < 10^{-3}$). Such loading is called "high-cyclic" or "poly-cyclic". It is of importance in many practical cases where the serviceability of a foundation is the main concern (e.g. on-shore or off-shore wind power plants, railways, watergates, tanks, machine foundations). Some structures are extremely sensitive to differential settlements, which must be kept within an extremely small range in order to ensure the operational requirements. In this case an accurate prediction of the residual deformations is required for several decades of operation.

For predictions of the accumulation of settlements due to a high-cyclic loading by means of the finite element (FE) method two different numerical strategies are combined. They are termed the *implicit* (conventional, low-cycle) and the *explicit* (N-type, high-cycle) mode of calculation. Time integration schemes (Euler forward / backward) are not meant here.

A conventional *pure implicit* calculation (Fig. 1a) with a $\dot{\sigma}$ - $\dot{\varepsilon}$ constitutive model (e.g. elastoplastic multi-surface models [4, 5, 22], endochronic models [38] or hypoplastic models with intergranular strain [24, 39]) is suitable only for small numbers of cycles ($N < 50$). For large N -values the numerical error becomes excessive in such calculations (Niemunis et al. [25]).

For a high-cyclic loading another strategy of calculation

ⁱ⁾Research Assistant, Institute of Soil Mechanics and Rock Mechanics, University of Karlsruhe, Germany (corresponding author). Email: torsten.wichtmann@ibf.uka.de

ⁱⁱ⁾Research Assistant, Institute of Soil Mechanics and Rock Mechanics, University of Karlsruhe, Germany

ⁱⁱⁱ⁾Professor and Director of the Institute of Soil Mechanics and Rock Mechanics, University of Karlsruhe, Germany

is necessary. It is illustrated in Fig. 1b for the case of a shallow foundation under cyclic loading. Only a few cycles are calculated *implicitly* with small increments $\dot{\sigma}(\dot{\varepsilon})\Delta t$ using a $\dot{\sigma}$ - $\dot{\varepsilon}$ constitutive model. Larger packages of cycles between are treated *explicitly*. The *explicit* mode requires a special constitutive formulation (so-called high-cycle accumulation (HCA) model) which takes packages of cycles ΔN as input. The accumulation of residual strain $\dot{\varepsilon}^{\text{acc}}\Delta N$ due to a package of ΔN cycles of a given strain amplitude $\varepsilon^{\text{ampl}}$ is treated similarly as a creep deformation due to time increments Δt in viscoplastic models. The number of cycles N just replaces the time t . Without tracing the oscillating strain path during the individual cycles, the explicit mode calculates directly the accumulation rate $\dot{\varepsilon}^{\text{acc}}$ which enters the constitutive equation (1).

The implicit parts of the calculation are necessary in order to determine the spatial field of the strain amplitude $\varepsilon^{\text{ampl}}$. The strain amplitude is an important input parameter for the HCA model (Section 2). The first cycle is *irregular* since the deformations in the first cycle can significantly differ from those in the subsequent cycles. Therefore the second cycle is used for the determination of $\varepsilon^{\text{ampl}}$. The strain amplitude is determined from the strain path $\varepsilon(t)$ recorded in each integration point during the second cycle. The procedure described by Niemunis et al. [25] is applied. During the explicit parts of the calculation the strain amplitude $\varepsilon^{\text{ampl}}$ is assumed constant. After several thousand cycles the spatial field of the strain amplitude may have changed due to a compaction and a re-distribution of stress. The explicit calculation should be therefore interrupted after definite numbers of cycles and $\varepsilon^{\text{ampl}}$ should be recalculated using the implicit mode (so-called *control cycles*, Fig. 1b).

For the development of a HCA model drained cyclic tests with a large number of cycles are necessary. The equations of the HCA model proposed by the authors (Niemu-

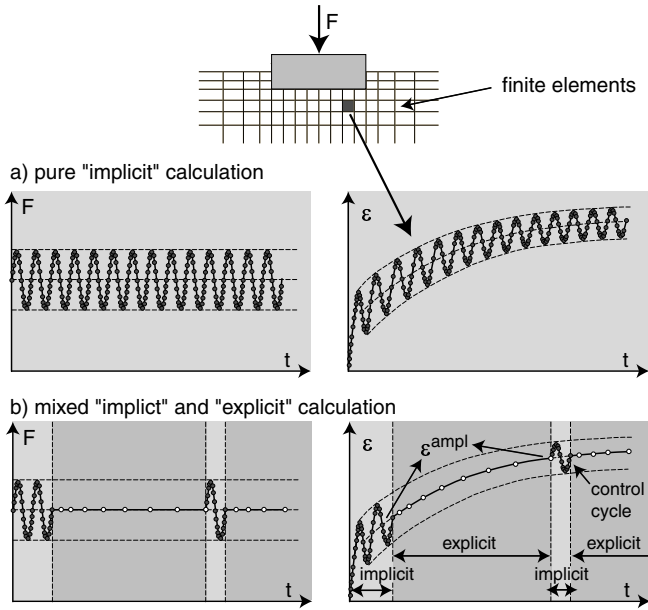


Fig. 1: FE calculation of the settlements of a shallow foundation under cyclic loading: a) Pure implicit versus b) combined implicit and explicit calculation

nis et al. [25], Section 2) have been developed based on numerous drained cyclic triaxial and cyclic multiaxial direct simple shear tests on a medium coarse to coarse uniform sand (No. 3 in Fig. 2). A detailed description of the test results can be consulted in [40–43]. These drained tests with a large number of cycles were necessary since most of the cyclic tests on sands documented in the literature have been performed under undrained conditions with focuss to the problem of liquefaction (e.g. Ishihara [13], Towhata [35]). Some studies (e.g. Silver & Seed [32], Youd [48], Tsukamoto et al. [36], Duku et al. [8]) with drained cyclic tests were dedicated to the residual deformations of partly saturated sand subjected to ground shaking during earthquakes. However, due to the limited number of cycles in these studies (e.g. $N = 15$ in [8]) the data cannot be used for the development of a HCA model. A survey of the literature discussing the influence of several parameters on the rate of strain accumulation in the drained case or the rate of pore water pressure in the undrained case has been given in [40, 41]. Deficits (lack of generality, missing influencing parameters, 1D formulation) of older HCA models proposed in the literature (e.g. Marr & Christian [19], Dyaljee & Raymond [7], Bouckovalas et al. [2], Sawicki & Świdziński [28, 29], Kagawa et al. [14], Gotschol [10]) have been discussed in [40]. The HCA model more recently proposed by Abdelkrim et al. [1] for ballast materials needs an experimental validation based on cyclic laboratory tests.

The present paper discusses the results of 200 drained cyclic triaxial tests on eight quartz sands with different grain size distribution curves. The tests have been performed due to the following reasons. First, the suitability of the equations of the HCA model for various kinds of sands and gravels should be examined. Second, a correlation of the material constants of the HCA model with granulometric properties (mean grain size d_{50} , coefficient of uniformity $U_c = d_{60}/d_{10}$) or index quantities (e.g. minimum void ratio e_{\min}) should be investigated. The aim was

to develop a simplified procedure for an estimation of a set of material constants. Furthermore, the test results offer the possibility to work out the influence of the grain size distribution curve on the accumulation of permanent strain due to a high-cyclic loading.

2 High-cycle accumulation model

The basic assumption of the HCA model proposed by Niemunis et al. [25] is that the strain path and the stress path that result from a cyclic loading can be decomposed into an oscillating part and a trend. The oscillating part is described by the strain amplitude. The HCA model predicts the trend (accumulation) of strain $\dot{\epsilon}^{\text{acc}}$ only. Depending on the boundary conditions, the trend of stress (pseudo-relaxation) or of strain (pseudo-creep) can be observed. They are interrelated by

$$\dot{\sigma} = E : (\dot{\epsilon} - \dot{\epsilon}^{\text{acc}} - \dot{\epsilon}^{\text{pl}}) \quad (1)$$

with the stress rate $\dot{\sigma}$ of the effective stress σ (compression positive), the strain rate $\dot{\epsilon}$ (compression positive), the given accumulation rate $\dot{\epsilon}^{\text{acc}}$, a plastic strain rate $\dot{\epsilon}^{\text{pl}}$ (for stress paths touching the yield surface, see Niemunis et al. [25]) and the barotropic elastic stiffness E . In the context of HCA models "rate" means a derivative with respect to the number of cycles N (instead of time t), i.e. $\dot{\square} = \partial \square / \partial N$. For $\dot{\epsilon}^{\text{acc}}$ in Eq. (1) the following expression is used:

$$\dot{\epsilon}^{\text{acc}} = \dot{\epsilon}^{\text{acc}} \mathbf{m} \quad (2)$$

with the flow rule $\mathbf{m} = \dot{\epsilon}^{\text{acc}} / \|\dot{\epsilon}^{\text{acc}}\| = (\dot{\epsilon}^{\text{acc}})^{\rightarrow}$ (unit tensor) and the flow intensity $\dot{\epsilon}^{\text{acc}} = \|\dot{\epsilon}^{\text{acc}}\|$. The superposed arrow denotes Euclidean normalization. The flow rule of the modified Cam clay (MCC) model is used for \mathbf{m} :

$$\mathbf{m} = \left[\frac{1}{3} \left(p - \frac{q^2}{M^2 p} \right) \mathbf{1} + \frac{3}{M^2} \boldsymbol{\sigma}^* \right]^{\rightarrow} \quad (3)$$

Although it significantly overestimates the Jaky's formula $K_0 = 1 - \sin \varphi$ for monotonic 1D compression, it approximates well the ratios $\dot{\epsilon}_v^{\text{acc}} / \dot{\epsilon}_q^{\text{acc}}$ measured in drained cyclic triaxial tests with $\dot{\epsilon}_v = \dot{\epsilon}_1 + 2\dot{\epsilon}_3$ and $\dot{\epsilon}_q = 2/3(\dot{\epsilon}_1 - \dot{\epsilon}_3)$ being the rates of volumetric or deviatoric strain, respectively. The superposed star \square^* denotes the deviatoric part of \square and p, q are Roscoe's invariants. For the triaxial case $p = (\sigma_1 + 2\sigma_3)/3$ and $q = \sigma_1 - \sigma_3$ holds. For triaxial extension ($\eta = q/p < 0$) a small modification $M = F M_c$ is used with

$$F = \begin{cases} 1 + M_e/3 & \text{for } \eta \leq M_e \\ 1 + \eta/3 & \text{for } M_e < \eta < 0 \\ 1 & \text{for } \eta \geq 0 \end{cases} \quad (4)$$

wherein

$$M_c = \frac{6 \sin \varphi_c}{3 - \sin \varphi_c} \quad \text{and} \quad M_e = -\frac{6 \sin \varphi_c}{3 + \sin \varphi_c}. \quad (5)$$

φ_c is the critical friction angle.

The intensity of strain accumulation $\dot{\epsilon}^{\text{acc}}$ in Eq. (2) is calculated as a product of six functions:

$$\dot{\epsilon}^{\text{acc}} = f_{\text{ampl}} \dot{f}_N f_e f_p f_Y f_{\pi} \quad (6)$$

Each function (see Table 1) considers the influence of a different parameter.

Influencing parameter	Function	Material constants	Reference quantities
Strain amplitude	$f_{\text{ampl}} = \min \left\{ \left(\frac{\varepsilon^{\text{ampl}}}{\varepsilon_{\text{ref}}^{\text{ampl}}} \right)^2 ; 100 \right\}$		$\varepsilon_{\text{ref}}^{\text{ampl}} = 10^{-4}$
Cyclic preloading	$\dot{f}_N = \dot{f}_N^A + \dot{f}_N^B$ $\dot{f}_N^A = C_{N1} C_{N2} \exp \left[-\frac{g^A}{C_{N1} f_{\text{ampl}}} \right]$ $\dot{f}_N^B = C_{N1} C_{N3}$	C_{N1}, C_{N2}, C_{N3}	
Average mean pressure	$f_p = \exp \left[-C_p \left(\frac{p^{\text{av}}}{p_{\text{ref}}} - 1 \right) \right]$	C_p	$p_{\text{ref}} = p_{\text{atm}} = 100 \text{ kPa}$
Average stress ratio	$f_Y = \exp (C_Y Y^{\text{av}})$	C_Y	
Void ratio	$f_e = \frac{(C_e - e)^2}{1 + e} \frac{1 + e_{\text{ref}}}{(C_e - e_{\text{ref}})^2}$	C_e	$e_{\text{ref}} = e_{\text{max}}$

Table 1: Summary of the functions, material constants and reference quantities of the HCA model

The function f_{ampl} describes the proportionality between $\dot{\varepsilon}^{\text{acc}}$ and the square of the strain amplitude $(\varepsilon^{\text{ampl}})^2$. It is valid up to strain amplitudes $\varepsilon^{\text{ampl}} \approx 10^{-3}$. For larger strain amplitudes, the accumulation rate was observed to be almost independent of $\varepsilon^{\text{ampl}}$ [40]. Therefore $f_{\text{ampl}} = 100$ is specified as an upper boundary in Table 1. The HCA model is primarily devoted to small strain amplitudes $\varepsilon^{\text{ampl}} < 10^{-3}$.

The model incorporates a tensorial definition of the amplitude for multidimensional strain loops [25]. The importance of multidimensionality has been demonstrated by test results of Pyke et al. [27] or Wichtmann et al. [42]. The present paper discusses only uniaxial cycles. In that case the novel amplitude definition is equal to the conventional one (i.e. $\square^{\text{ampl}} = \frac{1}{2}(\square^{\text{max}} - \square^{\text{min}})$).

The increase of $\dot{\varepsilon}^{\text{acc}}$ with decreasing average mean pressure p^{av} at $\eta^{\text{av}} = \text{constant}$ and with increasing average stress ratio $\eta^{\text{av}} = q^{\text{av}}/p^{\text{av}}$ at $p^{\text{av}} = \text{constant}$ is captured by the functions f_p and f_Y , respectively. In the function f_Y the stress ratio is described by Y^{av} instead of η^{av} , using the function Y of Matsuoka & Nakai [20]:

$$\bar{Y} = \frac{Y - 9}{Y_c - 9} \quad \text{with} \quad Y_c = \frac{9 - \sin^2 \varphi_c}{1 - \sin^2 \varphi_c} \quad (7)$$

$$Y = -\frac{I_1 I_2}{I_3} = \frac{27(3 + \eta)}{(3 + 2\eta)(3 - \eta)} \quad (8)$$

The I_i in Equation (8) are the basic invariants of the effective stress σ .

The function f_e in Eq. (6) describes the increase of the rate $\dot{\varepsilon}^{\text{acc}}$ with increasing void ratio e . In the cyclic triaxial tests the curves $\varepsilon^{\text{acc}}(N)$ of the residual strain versus the number of cycles were found to run proportional to the function f_N :

$$f_N = C_{N1} [\ln(1 + C_{N2}N) + C_{N3}N]. \quad (9)$$

It consists of a logarithmic and a linear portion. The derivative with respect to N is

$$\dot{f}_N = \underbrace{\frac{C_{N1} C_{N2}}{1 + C_{N2}N}}_{\dot{f}_N^A} + \underbrace{C_{N1} C_{N3}}_{\dot{f}_N^B} \quad (10)$$

It can be splitted into a N -dependent portion \dot{f}_N^A and a constant portion \dot{f}_N^B . However, the number of cycles N alone is

not a suitable state variable for the quantification of cyclic preloading (hysteresis) since it contains no information about the intensity of the cycles in the past. For that reason, the preloading (hysteresis) variable g^A was introduced into the HCA model. It counts the cycles weighting them with their amplitude

$$g^A = \int f_{\text{ampl}} \dot{f}_N^A dN \quad (11)$$

Only the N -dependent portion of \dot{f}_N is considered for g^A . The function \dot{f}_N^A was re-formulated using g^A instead of N (Table 1). The HCA model with g^A is able to predict correctly the accumulation of strain due to packages of cycles with different amplitudes applied in different sequences (see e.g. tests of Kaggwa et al. [14], Wichtmann [40]). The model approximately obeys Miner's rule [21] known from fatigue mechanics of metals, that means the sequence of the packages of cycles is of no importance, which is in good accordance with the experiments presented in [40].

The factor f_π considers that a change of the polarization of the cycles, that means a change of the direction of the cyclic loading, leads to an increase of the rate of accumulation. The corresponding experiments are given in [40, 42] (see also Yamada & Ishihara [45]). A detailed description of f_π can be found in [25]. Due to the constant polarization of the cycles $f_\pi = 1$ holds for the triaxial tests presented herein.

Numerous experimental studies with drained or undrained cyclic tests on clean sands could not find an influence of the loading frequency on the accumulation of residual strain or of pore water pressure, respectively. The drained cyclic tests of Youd [48], Shenton [30] and Duku et al. [8] were performed with frequencies in the range 0.1 Hz $\leq f \leq 30$ Hz while the studies of Yoshimi & Oh-oka [47], Yasuda & Soga [46] and Tatsuoka et al. [34] with undrained cyclic tests covered the range from 0.05 Hz to 12 Hz. A negligible influence of the loading frequency was reported. The frequency-independence has also been confirmed by our drained cyclic tests with 0.05 $\leq f \leq 2$ Hz [41] wherein dynamic effects are negligible. Therefore, the HCA model needs not to consider the loading frequency as an influencing parameter.

The multiplicative approach for $\dot{\varepsilon}^{\text{acc}}$ in Eq. (6) was chosen heuristically and then to some extent confirmed exper-

imentally (Wichtmann [40], Wichtmann et al. [41,43]). For example, f_{ampl} was found valid for two different average stresses, one with triaxial compression ($p^{\text{av}} = 200$ kPa, $\eta^{\text{av}} = 0.75$) and the other one with triaxial extension ($p^{\text{av}} = 200$ kPa, $\eta^{\text{av}} = -0.5$). The function f_Y was confirmed for different average mean pressures $50 \text{ kPa} \leq p^{\text{av}} \leq 300 \text{ kPa}$ and the function f_p was found valid for different average stress ratios $-0.5 \leq \eta^{\text{av}} \leq 1.313$, although the constants C_p and C_Y may slightly vary.

Some subtle deficiencies of the HCA model have been discussed by Niemunis et al. [26].

The HCA model has been implemented as a user's material model (= fortran routine UMAT) for the commercial FE program ABAQUS. The purpose of UMAT is to update the stress and all user-defined state variables and to return the tangential stiffness. The UMAT has three modes of operation:

1. Implicit mode: UMAT delegates the calculation to the conventional "implicit" UMAT treated as a subordinated procedure. As the "implicit" UMAT we use a version of the hypoplastic constitutive model with the so-called intergranular strain [24,39]. The implicit mode is used to find the initial state equilibrium and to perform irregular cycles (e.g. the first cycle). The numerical implementation of hypoplasticity is discussed in [23].
2. Recording mode: UMAT works in the implicit mode (hypoplasticity) but additionally the strain path is memorized. Only a few characteristic states need to be recorded. For that purpose several filtering criteria are used to economise on the computer memory. The recording mode provides the input data for the calculation of the strain amplitude $\varepsilon^{\text{ampl}}$. This mode is used for the second cycle and for control cycles.
3. Pseudo-creep mode: UMAT calculates stress increments explicitly using Eq. (1). Before the first increment is executed in this mode, the amplitude $\varepsilon^{\text{ampl}}$ is evaluated from the recorded strain path according to the procedure described by Niemunis et al. [25]. The FE program redistributes stress in the course of equilibrium iteration and, depending on the boundary conditions, the accumulation results in settlements or in pseudo-relaxation.

The subroutine UMAT can recognize the modes of operation by the number of the step specified in the input file. For more details on the implementation of the HCA model it is referred to Niemunis et al. [25].

3 Test device, tested material and testing program

Four cyclic triaxial devices of similar construction (Wichtmann et al. [40,41]) were used for the present study. The axial load was applied with pneumatic loading systems and was measured inside the pressure cell below the specimen. The cell pressure was kept constant in the tests of the present study. For triaxial tests with a simultaneous variation of the axial and the lateral stress see Wichtmann et al. [40,42].

Cylindrical specimens (diameter $d = 10$ cm, height $h = 20$ cm) were prepared using the pluviation technique. After flushing with CO_2 they were saturated with de-aired

water. A back pressure of 200 kPa was used in all tests. The quality of saturation was checked by a determination of Skempton's B-value. $B > 0.98$ was achieved in almost all tests. Axial deformations were measured with a displacement transducer attached to the load piston. The system compliance was accounted for. It was determined in preliminary tests on a steel dummy. The axial deformations obtained in this manner were found (Rondon et al. [?]) to be quite similar to the values measured locally on specimens with a square cross section using LDTs (Goto et al. [9], Hoque et al. [12]). Volume changes were determined via the pore water using a pipette system and a differential pressure transducer.

The grain size distribution curves of the eight sands are given in Fig. 2. They were obtained from sieving of a natural quartz sand obtained from a sand pit near Dorsten, Germany. The grain shape is sub-angular and the specific weight is $\rho_s = 2.65 \text{ g/cm}^3$. The mean grain sizes d_{50} , the coefficients of uniformity $U_c = d_{60}/d_{10}$, the curvature indices $U'_c = d_{30}^2/(d_{10}d_{60})$ and the maximum and minimum void ratios e_{max} and e_{min} (determined according to German standard code DIN 18126) are summarized in Table 2. The sands or gravels Nos. 1 to 6 were rather uniform ($1.3 \leq U_c \leq 1.9$) having mean grain sizes in the range $0.15 \text{ mm} \leq d_{50} \leq 4.4 \text{ mm}$. The sands Nos. 7 and 8 were mixed in order to test better graded grain size distribution curves. The sands Nos. 3, 7 and 8 had similar mean grain sizes ($0.52 \text{ mm} \leq d_{50} \leq 0.55 \text{ mm}$) but different coefficients of uniformity ($1.8 \leq U_c \leq 4.5$). The HCA model was originally developed based on test results of the sand No. 3.

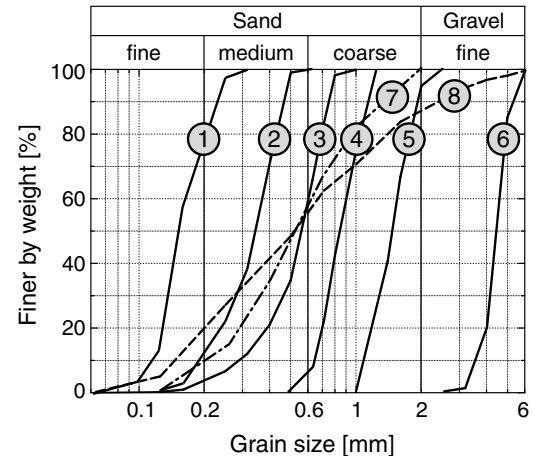


Fig. 2: Grain size distribution curves of the eight tested sands and gravels

For each sand four test series were performed. Throughout the tests of each series a single parameter of the HCA model (stress amplitude q^{ampl} , initial void ratio e_i , average mean pressure p^{av} or average stress ratio $\eta^{\text{av}} = q^{\text{av}}/p^{\text{av}}$) was varied while the remaining were kept constant. The effective stress paths are shown schematically in the p - q plane in Fig. 3. For each stress path, a new specimen was prepared (i.e. no multi-stage tests were performed). In the first series of tests (Fig. 3a) the stress amplitude q^{ampl} was varied between 10 and 90 kPa at $p^{\text{av}} = 200$ kPa and $\eta^{\text{av}} = 0.75$ (i.e. $\sigma_1^{\text{av}}/\sigma_3^{\text{av}} = 2$). The second series of tests (Fig. 3b)

Sand No.	1	2	3	4	5	6	7	8
d_{50} [mm]	0.15	0.35	0.55	0.84	1.45	4.4	0.55	0.52
$U_c = d_{60}/d_{10}$	1.4	1.9	1.8	1.4	1.4	1.3	3.2	4.5
$U'_c = d_{30}^2/(d_{10}d_{60})$	0.9	1.2	1.2	1.0	0.9	1.1	1.1	0.7
e_{\max}	0.992	0.930	0.874	0.878	0.886	0.851	0.811	0.691
e_{\min}	0.612	0.544	0.577	0.572	0.574	0.622	0.453	0.383
φ_c [°]	32.0	32.7	31.2	32.9	33.2	37.2	33.1	34.2

Table 2: Mean grain sizes d_{50} , coefficients of uniformity $U_c = d_{60}/d_{10}$, curvature indices $U'_c = d_{30}^2/(d_{10}d_{60})$, void ratios in loosest (e_{\max}) and densest (e_{\min}) condition and critical friction angles φ_c of the eight tested sands

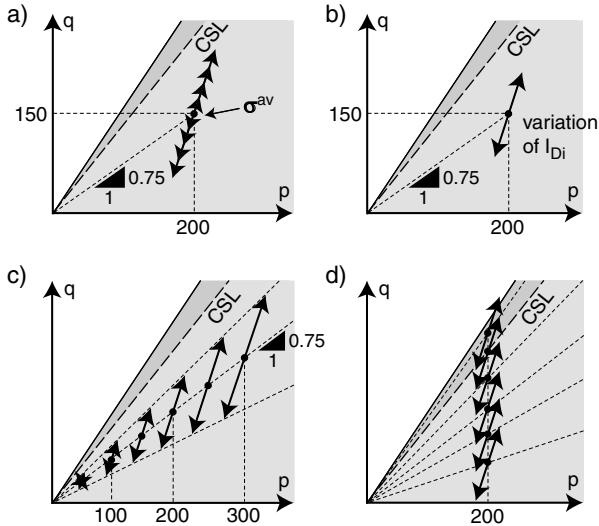


Fig. 3: Effective stress cycles in the four series of cyclic triaxial tests performed on each sand tests with a) different deviatoric stress amplitudes q^{ampl} , b) different initial relative densities I_{Di} , c) different average mean pressures p^{av} at a constant average stress ratio $\eta^{\text{av}} = q^{\text{av}}/p^{\text{av}}$ and d) different average stress ratios η^{av} at a constant value of p^{av}

in which the initial relative density

$$I_{Di} = \frac{e_{\max} - e_i}{e_{\max} - e_{\min}} = D_{ri} \frac{\varrho_{d,\max}}{\varrho_d} \quad (12)$$

was varied was performed at the same σ^{av} and with the same stress amplitude. In the third series (Fig. 3c) different average mean pressures between 50 kPa and 300 kPa were tested while the average stress ratio was $\eta^{\text{av}} = 0.75$. The amplitude-pressure ratio $\zeta = q^{\text{ampl}}/p^{\text{av}}$ was also kept constant within the series. The fourth series of tests (Fig. 3d) was performed with constant values of $p^{\text{av}} = 200$ kPa and q^{ampl} but with different average stress ratios $0.25 \leq \eta^{\text{av}} \leq 1.3$. The amplitude ratios $\zeta = q^{\text{ampl}}/p^{\text{av}}$ for the second, third and fourth test series were chosen between 0.15 and 0.4. It was lower for the sands showing larger accumulation rates.

After the application of the average stress and a resting period of 1 hour, the cyclic loading was commenced. The first *irregular* cycle was applied with a low frequency $f = 10$ mHz. Subsequently, 100,000 *regular* cycles with a frequency of 1 Hz were applied in all tests. A typical load pattern is given in Fig. 4. It shows the axial effective stress $\sigma_1(t)$ and the resulting axial strain $\varepsilon_1(t)$ during the first nine regular cycles of a test with $f = 1$ Hz and with a stress amplitude $q^{\text{ampl}} = 60$ kPa. The data were recorded during the first

25 cycles and during five cycles at $N = 50, 100, 200, 500, \dots, 5 \cdot 10^4$ and 10^5 .

Some sands (Nos. 2,3,5,8) were tested more extensively than the others (Nos. 1,4,6,7). The number of tests on the former ones was higher.

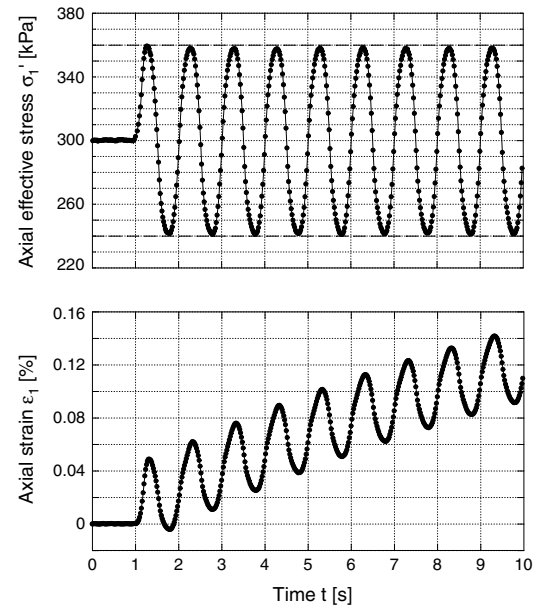


Fig. 4: Typical initial phase of a test: Axial effective stress σ_1 and axial strain ε_1 as a function of time t during the first nine regular cycles, test on sand No. 1 with $f = 1$ Hz, $p^{\text{av}} = 200$ kPa, $\eta^{\text{av}} = 0.75$ and $q^{\text{ampl}} = 60$ kPa

4 Test results

The HCA model does not describe the accumulation due to the *irregular* first cycle. Therefore, the data of this cycle is excluded from the diagrams presented in this paper. In the following, $N = 1$ denotes the state after the first *regular* cycle. The discussion of the test results concerns first the *direction* of accumulation $\dot{\varepsilon}_q^{\text{acc}}/\dot{\varepsilon}_v^{\text{acc}}$ (flow rule) and second its *intensity* $\dot{\varepsilon}^{\text{acc}}$.

4.1 Direction of strain accumulation

Fig. 5 justifies using the flow rule in the HCA model as a function of the average stress ratio η^{av} only. The accumulated deviatoric strain $\varepsilon_q^{\text{acc}}$ is plotted versus the accumulated volumetric strain $\varepsilon_v^{\text{acc}}$. Four test series regarding the influence of 1) amplitude, 2) relative density, 3) average mean pressure and 4) average stress ratio are shown for different sands. For a certain influencing parameter the diagrams for all tested sands look similar and therefore only

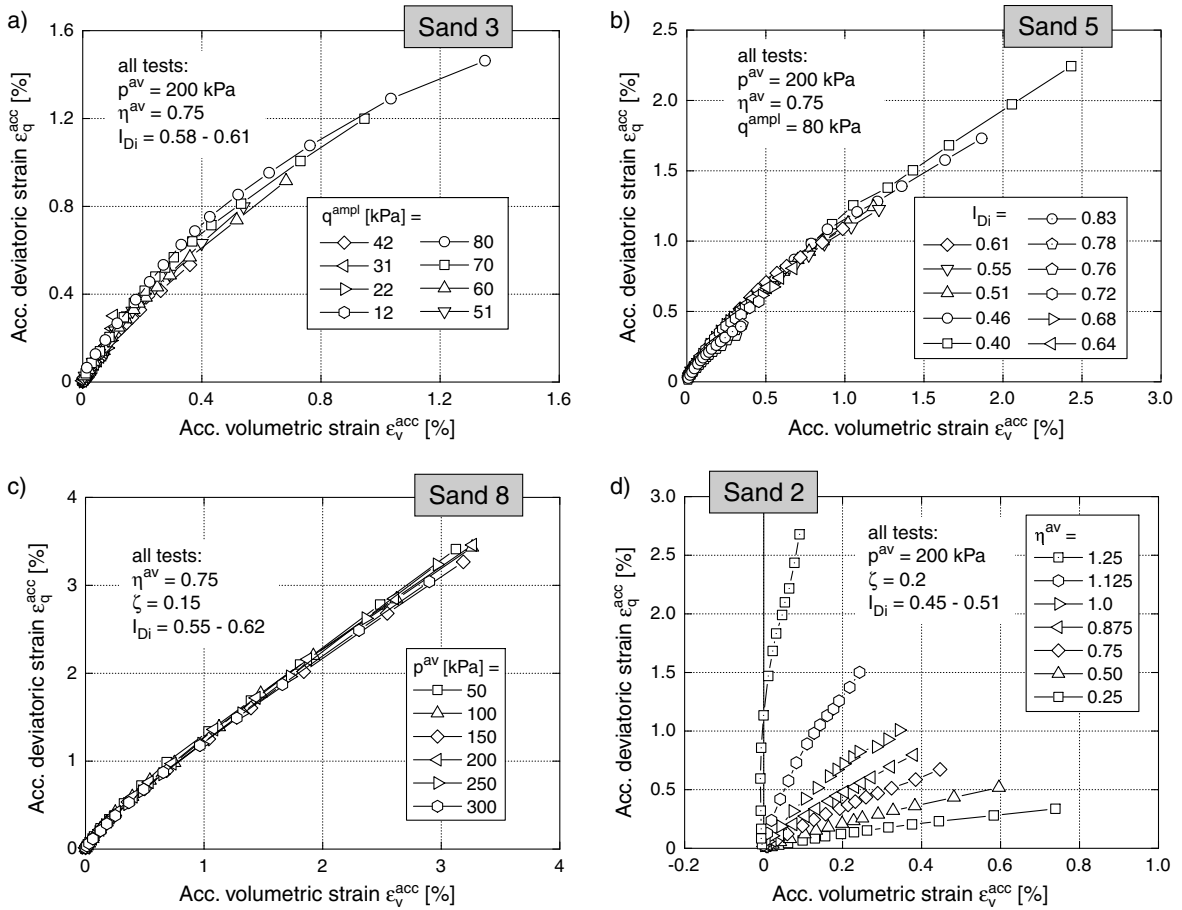


Fig. 5: $\varepsilon_q^{\text{acc}}-\varepsilon_v^{\text{acc}}$ -strain paths for different a) stress amplitudes q^{ampl} , b) initial relative densities I_{D_i} , c) average mean pressures p^{av} and d) average stress ratios η^{av}

the results for one sand (chosen more or less arbitrarily) are presented in Fig. 5. As obvious from Fig. 5, the direction of the $\varepsilon_q^{\text{acc}}-\varepsilon_v^{\text{acc}}$ -strain paths is only marginally influenced by the amplitude, the relative density and the average mean pressure (Fig. 5a-c). The most important influencing parameter is the average stress ratio $\eta^{\text{av}} = q^{\text{av}}/p^{\text{av}}$ (Fig. 5d). With increasing value of η^{av} , the ratio $\varepsilon_q^{\text{acc}}/\varepsilon_v^{\text{acc}}$ increases and \mathbf{m} becomes more deviatoric. As demonstrated in [43], a pure volumetric accumulation ($\varepsilon_q^{\text{acc}} = 0$) is observed at an isotropic average stress ($\eta^{\text{av}} = 0$, not tested in the present study). It is pure deviatoric ($\varepsilon_v^{\text{acc}} = 0$) at a critical stress ratio $\eta^{\text{av}} \approx M_c$ with M_c being the inclination determined from monotonic tests. At $\eta^{\text{av}} < M_c$ the cycles cause compaction while at $\eta^{\text{av}} > M_c$ dilatancy occurs (test at $\eta^{\text{av}} = 1.3$ on sand No. 3).

A slight increase of the volumetric portion of \mathbf{m} with N was observed in almost all tests. It becomes clear from Fig. 6 which shows the direction of strain accumulation as a vector in the p - q -plane. The vectors start at the average stress $\boldsymbol{\sigma}^{\text{av}}$ of a test and have an inclination of $\varepsilon_q^{\text{acc}}/\varepsilon_v^{\text{acc}}$ towards the horizontal. Different N -values are distinguished by different grayscales. The rotation of the vectors towards the positive p -axis with increasing number of cycles is obvious. Similar findings were also reported by Suiker et al. [33] for large stress cycles. Possible explanations of the N -dependence are discussed in [40].

Fig. 7 shows the ratios $\varepsilon_v^{\text{acc}}/\varepsilon_q^{\text{acc}}$ after 10^5 cycles as a function of η^{av} for the eight tested sands. The curves bound-

ing the shadowed area were calculated from the flow rule $\varepsilon_v^{\text{acc}}/\varepsilon_q^{\text{acc}} = (M_c - \eta^{\text{av}})^2/(2\eta^{\text{av}})$ of the modified Cam clay (MCC) model using the two extreme φ_c -values specified in Table 2. The critical friction angles of the eight materials were determined as the inclination of a pluviated cone. Since most of the data points in Fig. 7 fall within the shadowed area, a quite good approximation of the direction of accumulation by the MCC flow rule can be attested. Therefore, it is legitimate to use this flow rule in a HCA model (disregarding the small N -dependence).

The test results are in good accordance with earlier works of Luong [18] and Chang & Whitman [6] who also tested *small* stress cycles (but with a much lower maximum numbers of cycles). For *large* stress amplitudes with $q^{\text{min}} \approx 0$ and q^{max} approaching the failure line, as sometimes tested in pavement engineering (Suiker et al. [33]), the flow rule $\varepsilon_v^{\text{acc}}/\varepsilon_q^{\text{acc}}$ depends on the strain accumulated while the stress path is resting on the failure line (within a single cycle). Niemunis et al. [25] discussed how to handle this special case in a HCA model.

4.2 Intensity of strain accumulation

4.2.1 Strain amplitude

The accumulation curves $\varepsilon^{\text{acc}}(N)$ (with $\varepsilon = \sqrt{(\varepsilon_1)^2 + 2(\varepsilon_3)^2}$) for different stress amplitudes q^{ampl} are given in Fig. 8. The shape of these curves is discussed in Section 4.2.5. As already reported (e.g. Youd [48],

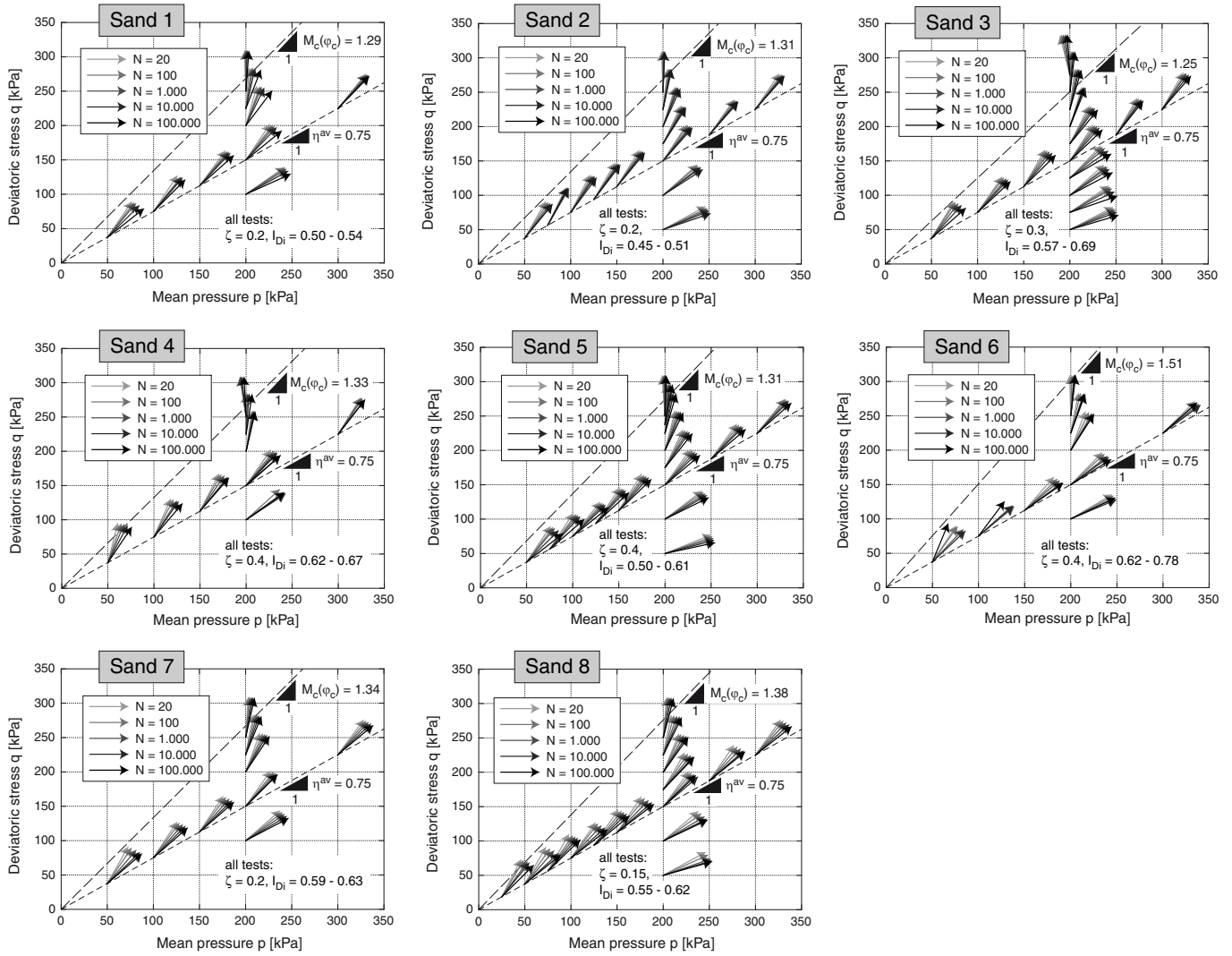


Fig. 6: Direction of strain accumulation shown as vectors in the p - q -plane. The vectors start at the average stress σ^{av} and have an inclination of $\varepsilon_q^{acc}/\varepsilon_v^{acc}$ towards the horizontal

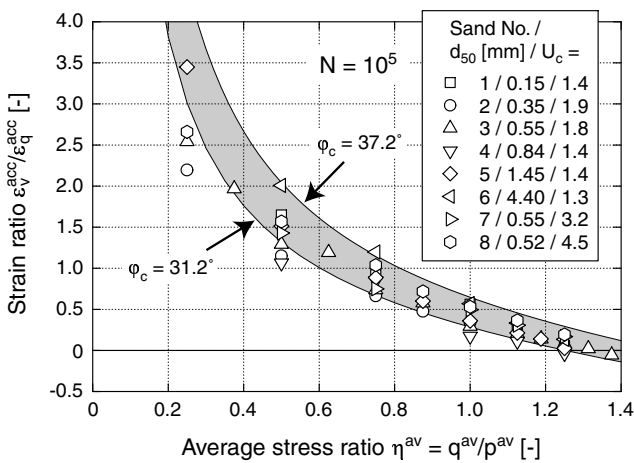


Fig. 7: Ratio $\varepsilon_v^{acc}/\varepsilon_q^{acc}$ after 10^5 cycles as a function of the average stress ratio η^{av}

Silver & Seed [31,32], Sawicki & Świdziński [28,29], Marr & Christian [19], Duku et al. [8]), the accumulation rate $\dot{\varepsilon}^{acc}$ increases with the stress amplitude. This is also

evident from Fig. 9 in which ε^{acc} caused by $N = 10^5$ cycles is given as a function of the stress amplitude q^{ampl} . For $q^{ampl} = \text{constant}$, the rate of strain accumulation tends to decrease with increasing mean grain size d_{50} . Furthermore, Fig. 9 shows that ε^{acc} significantly increases with the coefficient of uniformity U_c . A possible influence of the slightly different initial relative densities is discussed in the next section.

The HCA model is formulated with the strain amplitude ε^{ampl} as a driving parameter. In the stress-controlled tests the strain amplitude ε^{ampl} used to decrease during the first 100 cycles (at least for the larger stress amplitudes) and remained almost constant for $N > 100$. This is shown exemplarily for sand No. 3 in Fig. 10. Plotting the mean value $\bar{\varepsilon}^{ampl}$ over the 10^5 cycles as a function of the stress amplitude q^{ampl} , almost linear curves are obtained [41].

The function f_{ampl} of the HCA model assumes proportionality between $\dot{\varepsilon}^{acc}$ and the square of the strain amplitude $(\varepsilon^{ampl})^2$. In order to verify this assumption, the diagrams in Fig. 11 were generated for the eight tested sands. They show the residual strain ε^{acc} after different numbers of cycles as a function of the square of the strain amplitude $(\bar{\varepsilon}^{ampl})^2$. The bar over a symbol \sqcup denotes that a

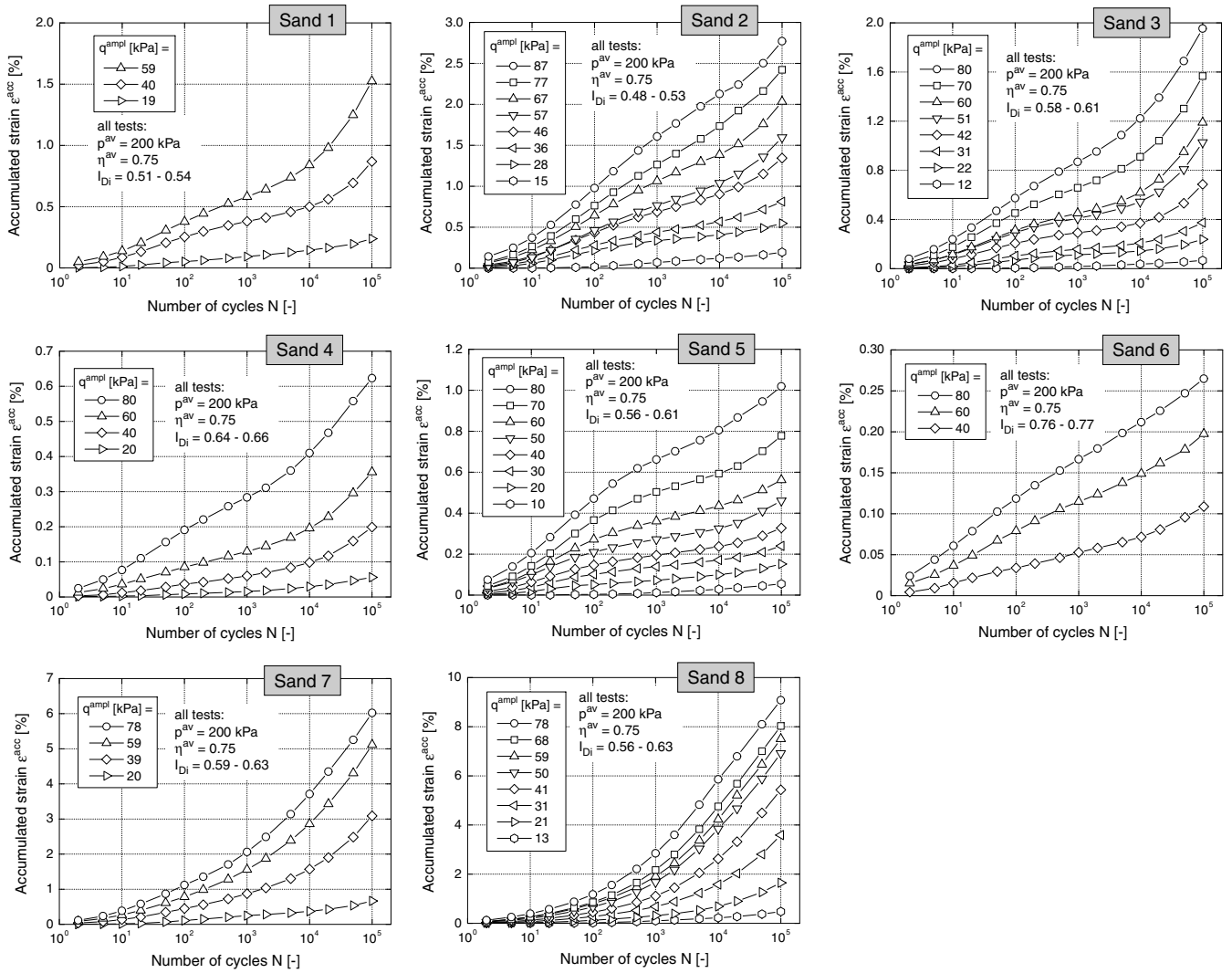


Fig. 8: Accumulation curves $\varepsilon^{acc}(N)$ in the tests with different stress amplitudes q^{ampl}

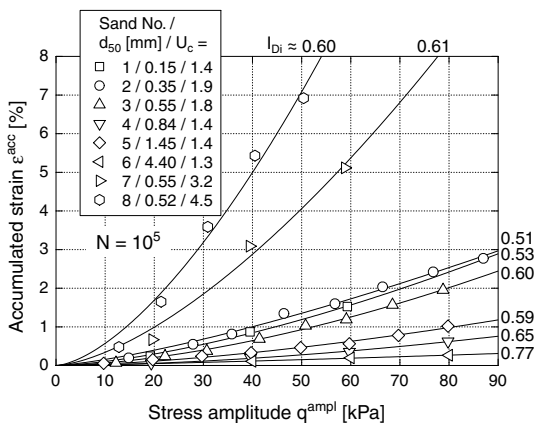


Fig. 9: Accumulated strain ε^{acc} after 10^5 cycles as a function of the stress amplitude q^{ampl}

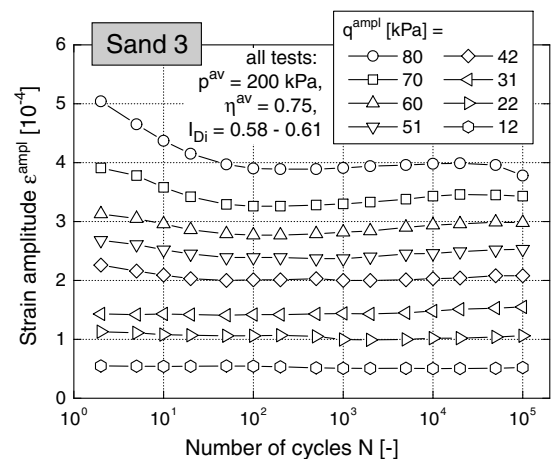


Fig. 10: Development of strain amplitude ε^{ampl} with the number of cycles

mean value over N is used, i.e. $\bar{\square} = (\int \square dN)/N$. On the y -axis the residual strain was divided by the void ratio function \bar{f}_e (discussed in the next section) in order to consider slightly different initial densities and different compaction rates. The linear curves through the origin in Fig. 11 con-

firm the function f_{ampl} . f_{ampl} is a proportionality factor between the rate $\dot{\varepsilon}^{acc}$ and $(\varepsilon^{ampl})^2$. If observed at constant values of ε^{ampl} , p^{av} , η^{av} , e and N , also the residual strain ε^{acc} should be proportional to $(\varepsilon^{ampl})^2$. In Fig. 11

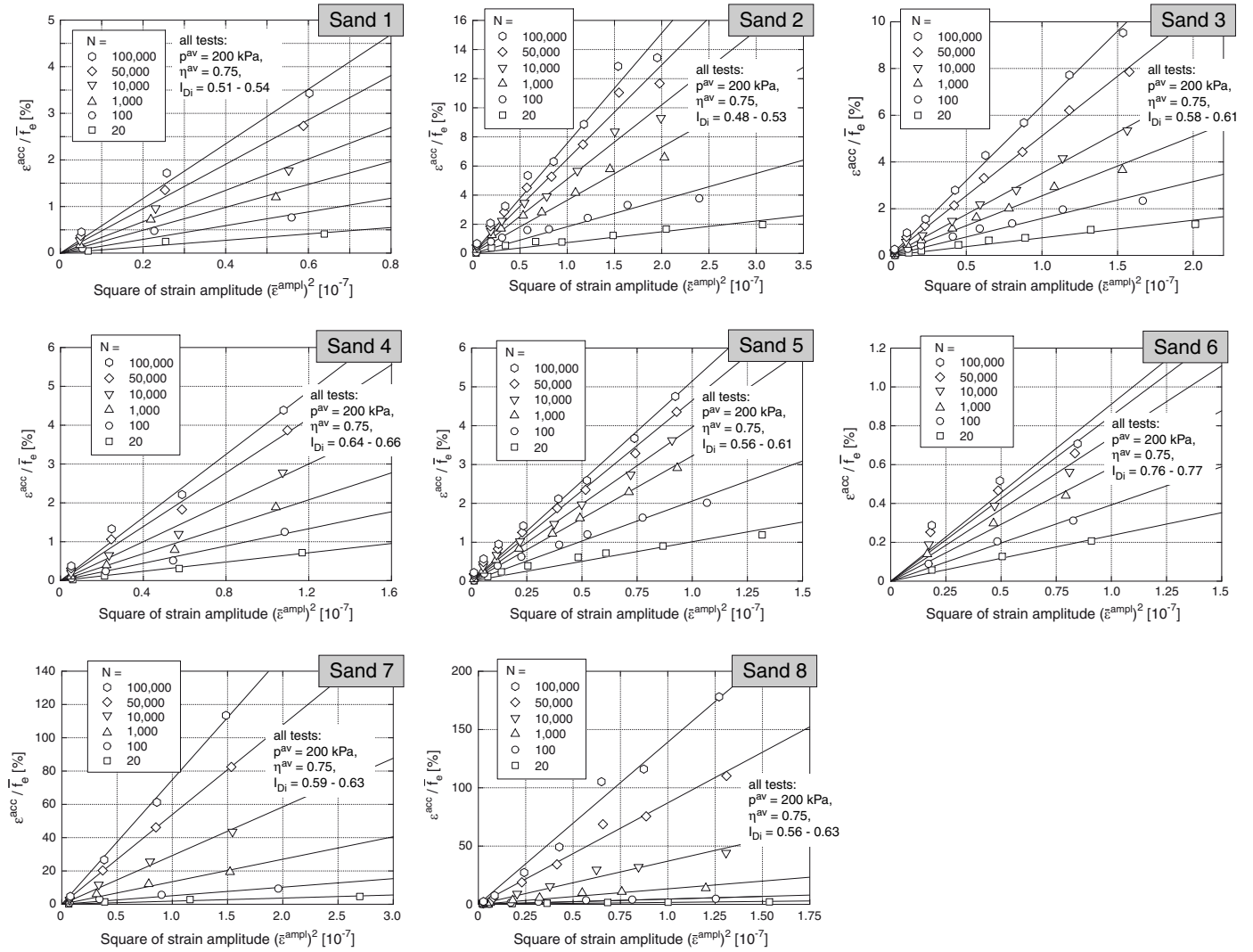


Fig. 11: Confirmation of the function f_{ampl} of the HCA model for the eight sands: Accumulated strain ϵ^{acc} divided by void ratio function \bar{f}_e plotted versus $(\epsilon^{ampl})^2$

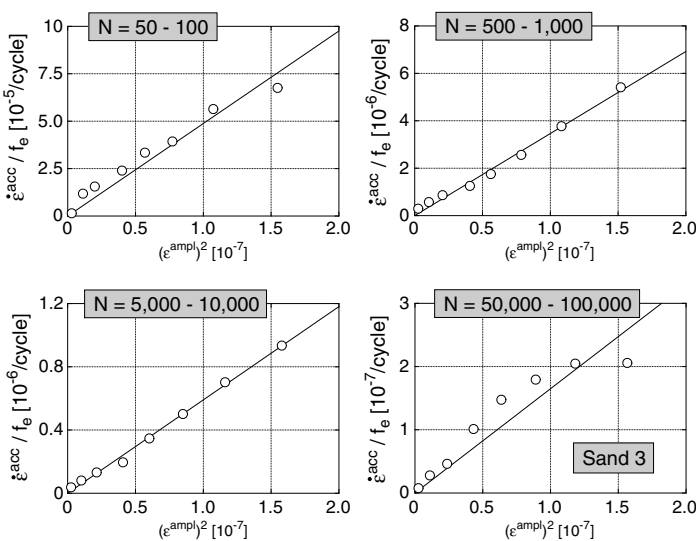


Fig. 12: Rates $\dot{\epsilon}^{acc} \approx \Delta\epsilon^{acc} / \Delta N$ divided by f_e as a function of the square of the strain amplitude $(\epsilon^{ampl})^2$, data from tests with different amplitudes on sand No. 3. ϵ^{ampl} and f_e are the mean values of two adjacent data recordings.

such "idealized" test conditions have been artificially created by dividing ϵ^{acc} by \bar{f}_e . The rate can be calculated as $\dot{\epsilon}^{acc} \approx \Delta\epsilon^{acc} / \Delta N$ with Δ denoting the differences in the variables between two data recordings. Plots of $\dot{\epsilon}^{acc}$ versus $(\epsilon^{ampl})^2$ for different N -values (Figure 12). also confirm f_{ampl} .

The exponent $a = 2$ of the relationship $\dot{\epsilon}^{acc} \sim (\epsilon^{ampl})^a$ is in good accordance with the triaxial data of Marr & Christian [19] ($1.9 \leq a \leq 2.3$). Sometimes lower values of the exponent a are reported from simple shear tests (e.g. a mean value $a = 1.2$ was obtained by Duku et al. [8]). It may be attributed to the large strain amplitudes in these tests.

4.2.2 Void ratio

Fig. 13 contains the accumulation curves $\epsilon^{acc}(N)$ of sand No. 5 for different initial relative densities. As expected and in accordance with earlier test results (Silver & Seed [31,32], Youd [48], Hain [11], Marr & Christian [19], Duku et al. [8]), the intensity of accumulation increases with decreasing initial relative density I_{Di} . Similar results have been obtained from the tests of the remaining seven sands.

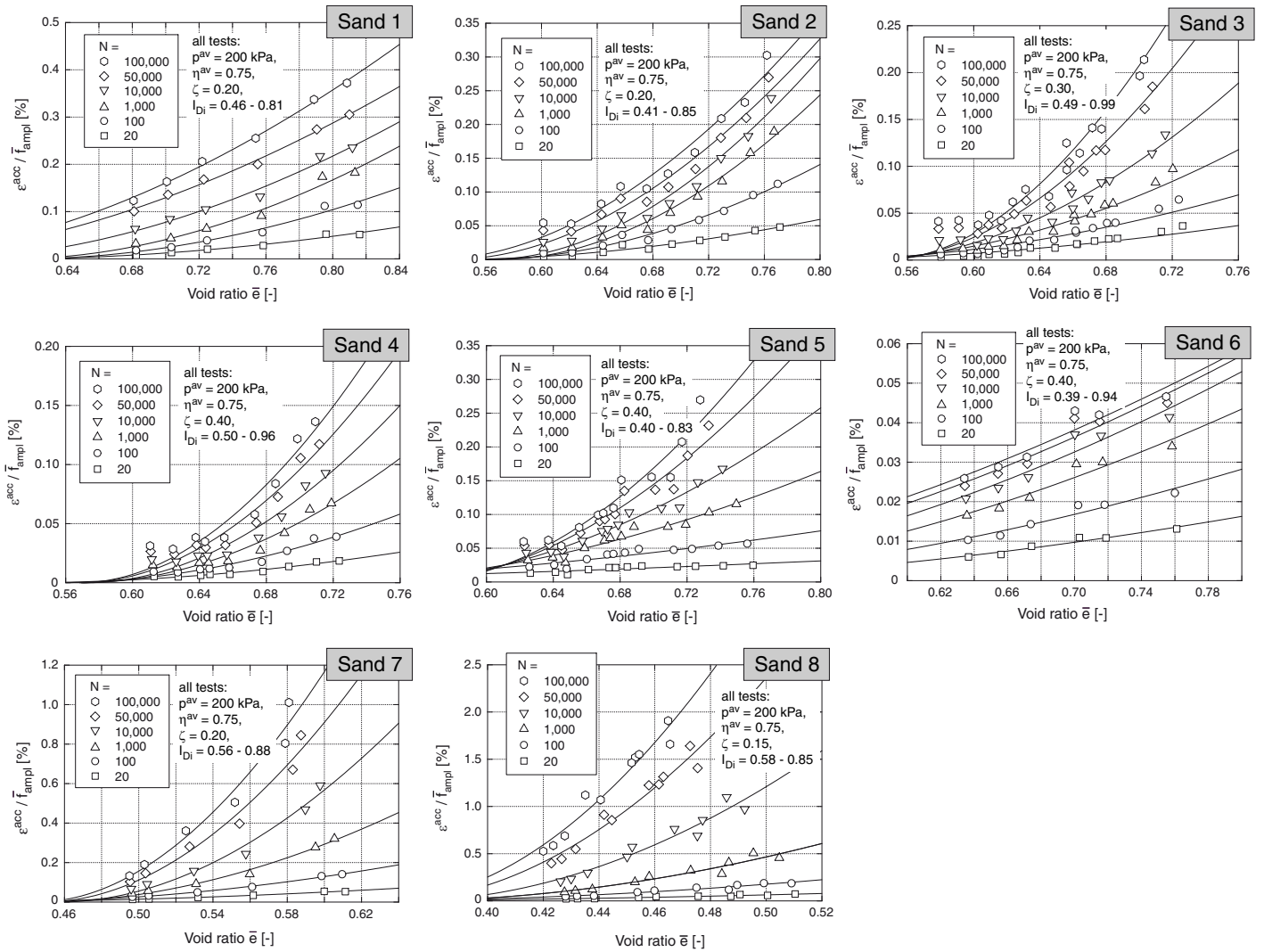


Fig. 14: Accumulated strain ϵ^{acc} divided by the amplitude function \bar{f}_{amp} versus a mean value \bar{e} of the void ratio, fitting of function f_e

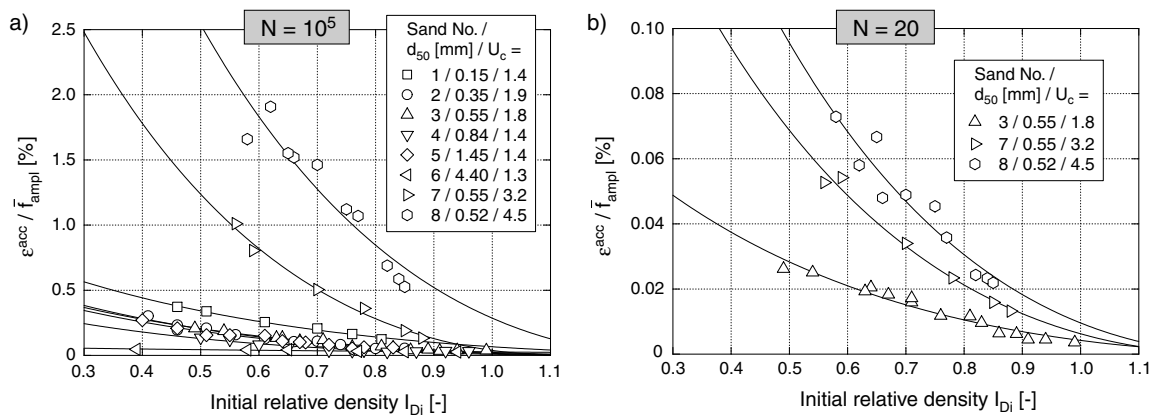


Fig. 15: Comparison of curves of normalized accumulated strain $\epsilon^{acc} / \bar{f}_{amp}$ versus initial relative density I_{Di} after a) $N = 10^5$ cycles and b) $N = 20$ cycles

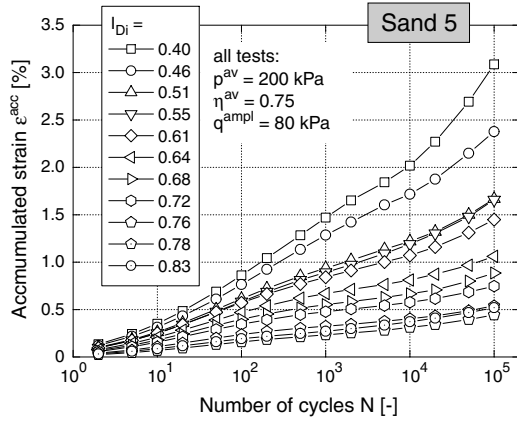


Fig. 13: Accumulation curves $\varepsilon^{\text{acc}}(N)$ in tests with different initial relative densities I_{D_i}

The residual strain as a function of N and \bar{e} is given in Fig. 14. The strain amplitude $\varepsilon^{\text{ampl}}$ slightly increases with increasing void ratio. In order to free the data from this influence, the accumulated strain ε^{acc} has been divided by the amplitude function \bar{f}_{ampl} . The bar over f_{ampl} denotes that the function was calculated with a mean value $\bar{\varepsilon}^{\text{ampl}}$ of the strain amplitude. The hyperbolic function f_e (Table 1) has been fitted to the data (curves in Fig. 14). The constant C_e is equal to the void ratio for which $\dot{\varepsilon}^{\text{acc}} = 0$ holds. Mean values of C_e are summarized in Table 3. For some of the sands, the function f_e seems to underestimate the accumulation rates at large densities. This needs a further investigation in future.

In Fig. 15a the residual strain ε^{acc} after 10^5 cycles is plotted versus the initial relative density I_{D_i} . Since the tests on the eight sands were performed with different stress amplitudes q^{ampl} , the ε^{acc} -values have been normalized by the amplitude function \bar{f}_{ampl} to ease the comparison. Comparing the data for the uniform sands Nos. 1 to 6, Fig. 15a reveals that for $I_{D_i} = \text{constant}$ the accumulation rate tends to increase with decreasing mean grain size d_{50} . Similar results were reported regarding the rate of pore water pressure accumulation in undrained cyclic tests (Lee & Fitton [16], Castro & Poulos [3]). Therefore, the differences of the ε^{acc} -values for sands Nos. 1 to 6 in Fig. 9 cannot be explained with differences in the I_{D_i} -values.

Furthermore, Fig. 15a confirms that the residual strains increase considerably with increasing coefficient of uniformity U_c of the tested sand. This is in contrast to the results of undrained cyclic tests performed on sands with different U_c -values (Vaid et al. [37], Kokusho et al. [15]). In those tests, no influence of U_c on the liquefaction resistance could be found if the specimens were prepared with similar relative densities. However, it is obvious from Fig. 15a that the U_c -independence for $I_D = \text{constant}$ seems not to apply to the accumulation of strain in drained cyclic tests. In order to study if the different findings from undrained tests are due to the smaller number of cycles, the diagram in Fig. 15b for $N = 20$ was plotted. Only the data for the sands Nos. 3, 7 and 8 with same values of d_{50} are given. Although the U_c -dependence in this data is slightly weaker than that observed for 10^5 (due to the different shape of the curves $\varepsilon^{\text{acc}}(N)$ for uniform and well-graded sands, Section 4.2.5), the accumulation rates of the three sands still differ significantly. The different results from undrained

tests may be attributed to the change of the average effective stress and the increase of the strain amplitude with increasing number of cycles N .

4.2.3 Average mean pressure

The accumulation curves $\varepsilon^{\text{acc}}(N)$ measured in the tests with a variation of p^{av} are given exemplarily for sand No. 8 in Fig. 16. In the tests with a constant amplitude-pressure ratio $\zeta = q^{\text{ampl}}/p^{\text{av}}$, the residual strain was almost independent of p^{av} for most of the tested sands. However, due to the stress-dependence of the secant stiffness, the strain amplitudes increase with increasing p^{av} at $\zeta = \text{constant}$ (Fig. 17).

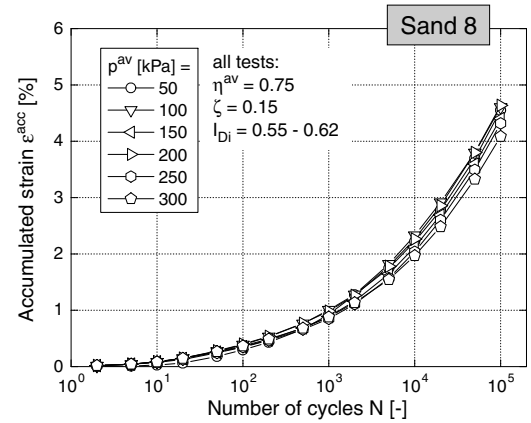


Fig. 16: Accumulation curves $\varepsilon^{\text{acc}}(N)$ in tests with different average mean pressures p^{av}

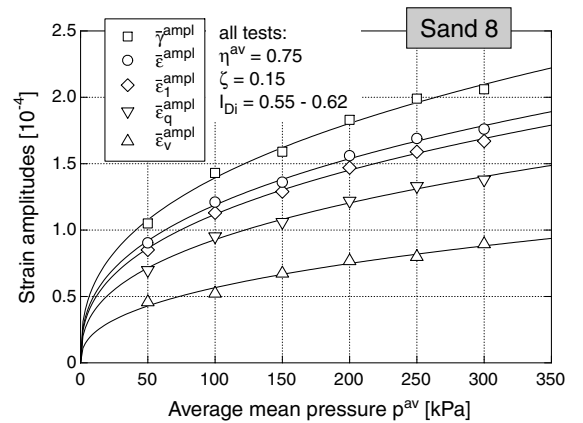


Fig. 17: Strain amplitudes $\varepsilon_1^{\text{ampl}}$, $\varepsilon_v^{\text{ampl}}$, $\varepsilon_q^{\text{ampl}}$, $\varepsilon^{\text{ampl}}$ and $\bar{\gamma}^{\text{ampl}}$ (mean values over 10^5 cycles, $\gamma = \varepsilon_1 - \varepsilon_3$) as a function of the average mean pressure p^{av}

The residual strain in Fig. 18 has been normalized by the amplitude function \bar{f}_{ampl} and by the void ratio function f_e . It is plotted versus p^{av} . From this diagram one can conclude that for $\varepsilon^{\text{ampl}} = \text{constant}$ and $e = \text{constant}$ the intensity of accumulation decreases with increasing average mean pressure for all sands. The exponentially decreasing function f_p (Table 1) has been fitted to the test data (curves in Fig. 18). The parameter C_p turns out to increase with N [41] which has not been implemented into the HCA model for sake of simplicity. In Table 3 the mean values of C_p over $N = 10^5$ cycles are presented. Furthermore, the function

Constant	Sand							
	1	2	3	4	5	6	7	8
C_e	0.57	0.55	0.54	0.56	0.54	0.38	0.44	0.36
e_{ref}	0.992	0.930	0.874	0.878	0.886	0.851	0.811	0.691
C_p	0.60	0.84	0.43	0.58	0.68	0.30	0.68	0.61
C_Y	1.8	2.7	2.0	2.8	2.8	3.0	2.2	3.1
C_{N1}	0.00087	0.00077	0.00036	0.00027	0.00043	0.000048	0.0044	0.0083
C_{N2}	0.22	0.27	0.43	0.38	0.32	1.27	0.029	0.0059
C_{N3}	0.00004	$7.4 \cdot 10^{-6}$	0.00005	0.00004	$7.0 \cdot 10^{-7}$	0	0.00005	0.00007

Table 3: Constants of the HCA model for the eight tested sands

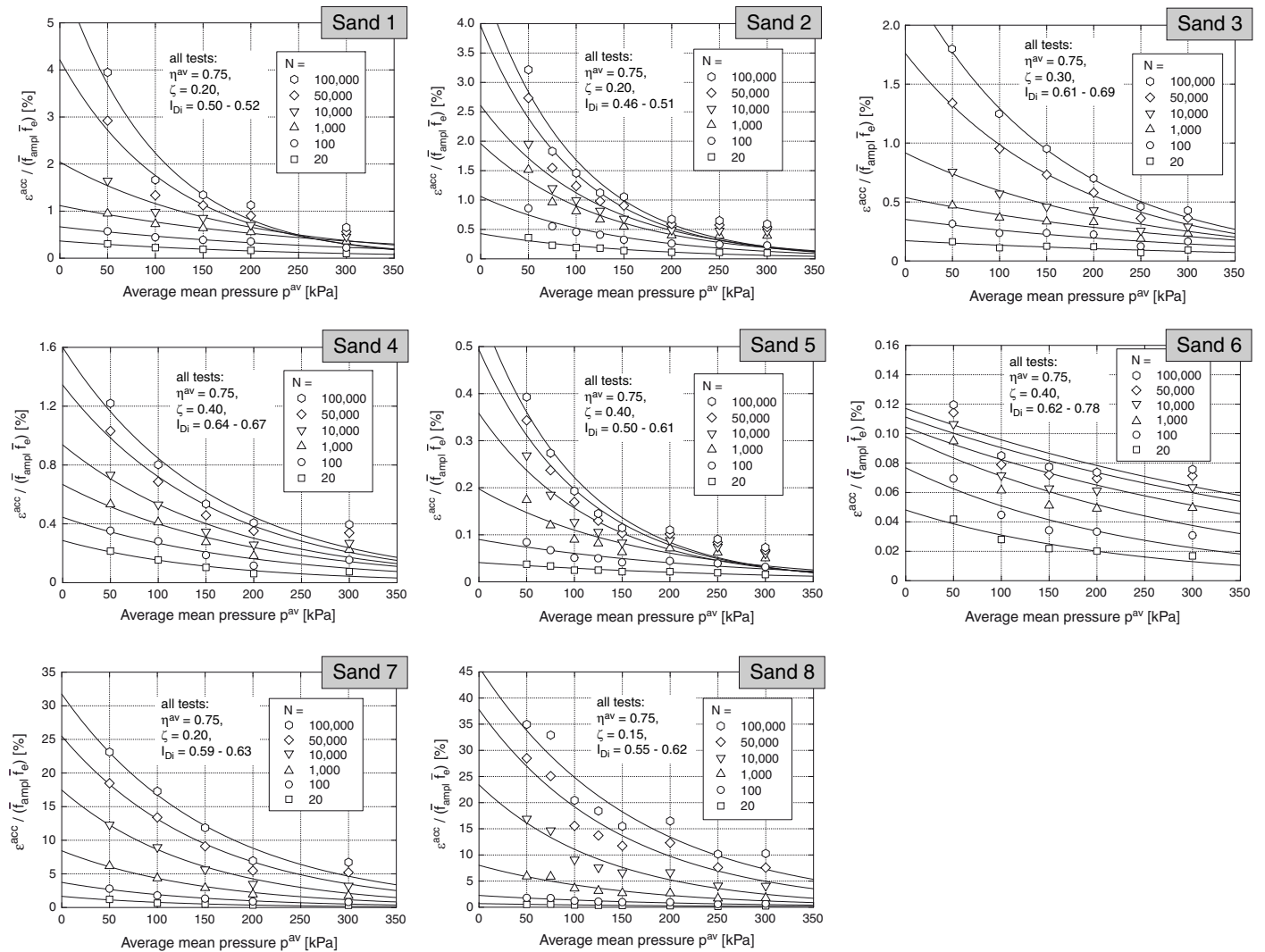


Fig. 18: Accumulated strain ϵ^{acc} divided by \bar{f}^{amp} and \bar{f}_e versus average mean pressures p^{av} , fitting of function f_p

f_p seems to underestimate the accumulation rates at larger pressures. A more detailed examination including larger pressures will be undertaken in future.

In the simple shear tests done by Silver & Seed [31,32], Youd [48] and Sawicki & Świdziński [28,29], no influence of the vertical stress on the accumulation of residual strain was observed, possibly due to the low number of cycles applied. Some materials (e.g. sand No. 3) used in the present study show also only a marginal p^{av} -dependence of ε^{acc} for low N -values. In contrast to the earlier studies, the more recent simple shear study of Duku et al. [8] found a significant decrease of the accumulation rate with increasing vertical stress, which is in good accordance with the present study. A micromechanical explanation has been provided by Duku et al. [8].

4.2.4 Average stress ratio

The accumulation curves $\varepsilon^{acc}(N)$ measured in tests with different average stress ratios η^{av} are given in Fig. 19, exemplarily for Sand No. 7. For a constant q^{ampl} the higher the η^{av} -values, the higher are the rates of accumulation. The strain amplitude ε^{ampl} slightly decreases with increasing stress anisotropy. In Fig. 20 the ε^{acc} -data for all sands were normalized by \bar{f}_e and \bar{f}_{ampl} and plotted versus the average stress ratio \bar{Y}^{av} . This illustration confirms that the intensity of accumulation increases with increasing \bar{Y}^{av} . A fitting of the exponential function f_Y (Table 1) to the data in Fig. 20 (curves) lead to the representative values of C_Y given in Table 3.

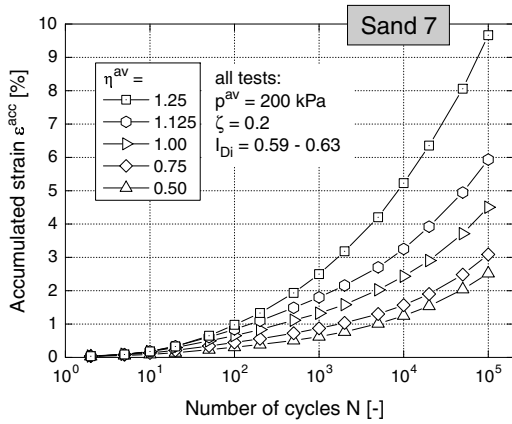


Fig. 19: Accumulation curves $\varepsilon^{acc}(N)$ in tests with different average stress ratios η^{av}

4.2.5 Number of cycles / cyclic preloading

The characteristic shape of the curves $\varepsilon^{acc}(N)$ can be seen in Figs. 8, 13, 16 and 19. For the uniform sands Nos. 1 to 6, the residual strain increases almost proportionally to $\ln(N)$ up to $N \approx 10^4$. It becomes overlogarithmic for larger N -values. For the sands Nos. 7 and 8, having higher U_c -values, the residual strain grows faster than according to $\varepsilon^{acc} \sim \ln N$ already from the beginning of the test. Some researchers (e.g. Lentz & Baladi [17], Duku et al. [8]) found accumulation curves obeying $\varepsilon^{acc}(N) \sim \ln(N)$ whereas other studies (e.g. Marr & Christian [19]) suggest an increase of ε^{acc} faster than proportional to $\ln(N)$. The results of the present study show, that these differences may

be due to the different grain size distribution curves of the tested materials. In particular, the shape of the accumulation curves $\varepsilon^{acc}(N)$ depends on the coefficient of uniformity U_c .

In Fig. 21 numerous curves $\varepsilon^{acc}(N)$ from the four test series have been normalized by the functions \bar{f}_{ampl} , \bar{f}_e , \bar{f}_p and \bar{f}_Y . Fitting of data in Fig. 21 with f_N (see Eq. (9)) provides the constants C_{N1} , C_{N2} and C_{N3} given in Table 3. For sand No. 4, the shape of the curves $\varepsilon^{acc}(N)$ at large stress ratios $\eta^{av} > 1$ differs from that at lower values of η^{av} . Based on the present data this effect cannot be explained or implemented into the HCA model yet. The respective curves are shown in Fig. 21 but have been neglected in the curve-fitting of f_N .

Tests with larger numbers of cycles ($N > 10^5$) are being performed at the moment in order to verify the applicability of the function f_N for larger N -s.

5 Prediction of the HCA model

Fig. 22 presents a comparison of the residual strain ε^{acc} measured in the cyclic triaxial tests with values predicted by the HCA model using the material constants summarized in Table 3. For each test, data for $N = 10^2, 10^3, 10^4$ and 10^5 are provided. For most tests, the data points plot close to the bisecting line. That means that the HCA model predicts quite well the ε^{acc} -values measured in the cyclic triaxial tests. However, for some of the tests there are larger deviations of the predicted from the measured values due to the shortcomings of the individual functions discussed above or due to the scatter of data shown in Fig. 21. Improvements to the prediction of the HCA model for these special cases seem feasible only at the cost of more complicated fitting functions.

6 Correlation of material constants with granulometric properties

The direct determination of the material constants of the HCA model from cyclic tests is quite laborious. The procedure has been explained in more detail by Wichtmann et al. [44]. At least nine cyclic triaxial tests are necessary and sophisticated test devices are indispensable. In order to develop a simplified procedure some correlations between the material constants of the HCA model and the granulometric properties d_{50} and U_c or with index properties (e.g. minimum void ratio e_{min}) have been investigated.

Fig. 23a presents C_e as a function of e_{min} . The correlation

$$C_e = 0.96 e_{min} \quad (13)$$

approximates well the data except for the fine gravel No. 6. The independence of C_p and C_Y of d_{50} and U_c is shown in Fig. 23b and 23c. Although linear functions could be justified, the choice of constant values

$$C_p = 0.59 \quad \text{and} \quad C_Y = 2.6 \quad (14)$$

is recommended at present due to the sparse data. The empirical correlation of C_{N1} , C_{N2} and C_{N3} with d_{50} and U_c (Fig. 23d-f) may be expressed as follows:

$$C_{N1} = 0.0002 \exp(-0.65 d_{50}) \exp(0.91 U_c) \quad (15)$$

$$C_{N2} = 0.95 \exp(0.33 d_{50}) \exp(-0.90 U_c) \quad (16)$$

$$C_{N3} = 0.00003 \exp(-0.69 d_{50}) \exp(0.26 U_c) \quad (17)$$

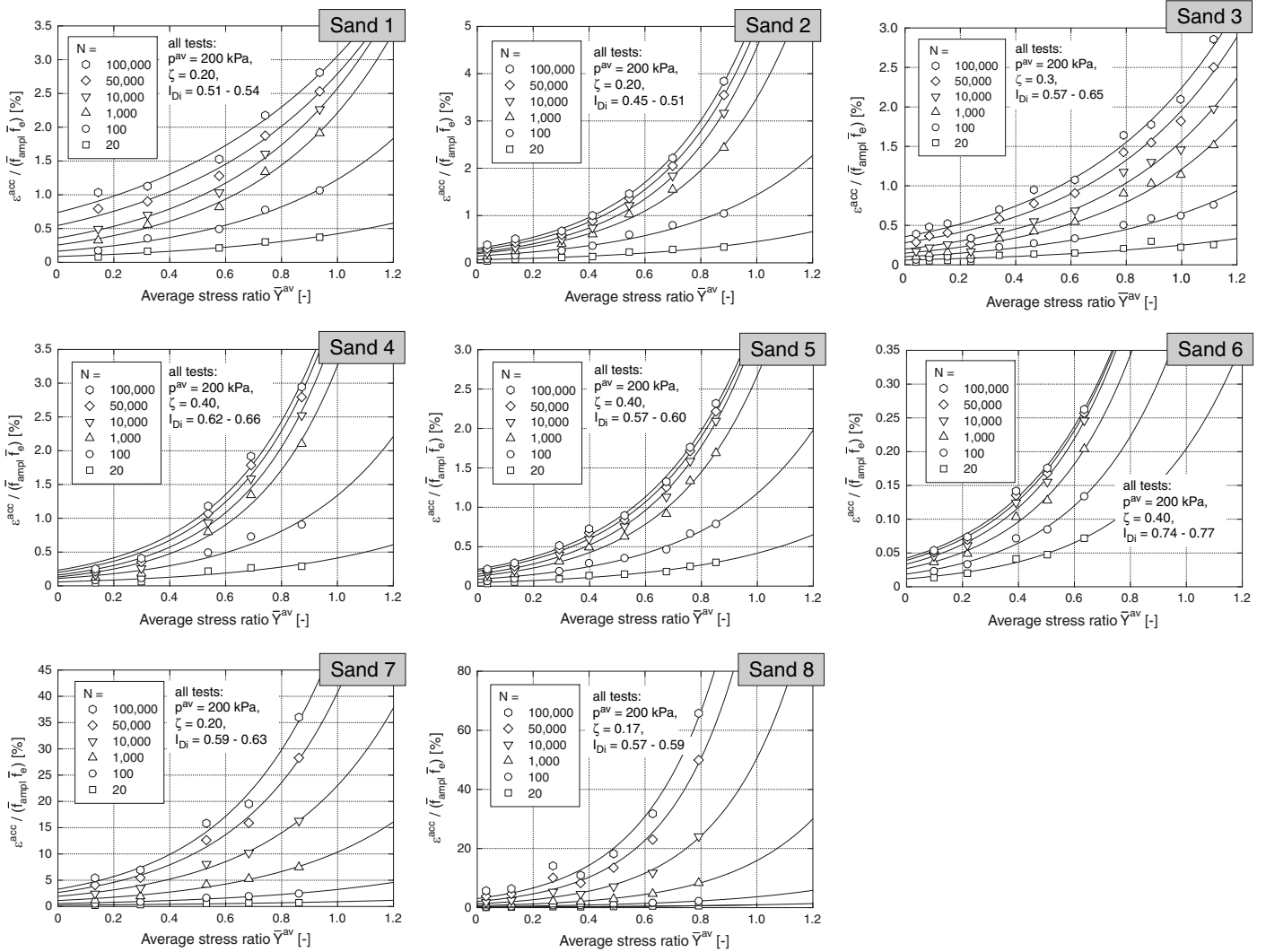


Fig. 20: Accumulated strain ϵ^{acc} divided by \bar{f}^{ampl} and \bar{f}_e versus average stress ratio \bar{Y}^{av} , fitting of function f_Y

The data of C_{N3} show a significant scatter. C_{N3} dictates the accumulation at large N -values and may be better determined from tests with larger numbers of cycles $N > 10^5$. Such tests are being performed at present.

A set of constants of the HCA model may be roughly estimated from Eqs. (13) to (17). If cyclic triaxial devices are available, a set of constants may be obtained with little effort by estimating C_e , C_p and C_Y from Eqs. (13) to (14) and by performing only one test in order to fit the constants C_{N1} to C_{N3} .

7 Summary, conclusions and outlook

The results of approx. 200 cyclic triaxial tests on eight quartz sands with different grain size distribution curves ($0.15 \text{ mm} \leq d_{50} \leq 4.4 \text{ mm}$, $1.3 \leq U_c \leq 4.5$) have been examined from the point of view of a high-cycle accumulation (HCA) model. The stress amplitude q^{ampl} , the initial relative density I_{Di} , the average mean pressure p^{av} and the average stress ratio $\eta^{av} = q^{av}/p^{av}$ have been varied in the tests. The applicability of a HCA model developed based on the results for a uniform medium coarse to coarse sand to the other sands and gravels is investigated. The test results confirmed the flow rule $\dot{\epsilon}_q^{acc}/\dot{\epsilon}_v^{acc}$ observed in earlier

experiments and derived as the associated flow rule of the modified Cam-clay (MCC) model. The proportionality between the intensity of accumulation $\dot{\epsilon}^{acc}$ and the square of the strain amplitude $(\epsilon^{ampl})^2$ was confirmed for all sands. Also the functions f_e , f_p , f_Y and f_N of the HCA model describing the dependence of the accumulation rate $\dot{\epsilon}^{acc}$ on void ratio, average mean pressure, average stress ratio and cyclic preloading were found useful for all of the eight tested sands. It was demonstrated that the HCA model with the material constants determined from the cyclic triaxial tests approximates quite well most of the accumulation rates measured in the laboratory. Correlations of the material constants of the HCA model with granulometric properties (d_{50} , U_c) or with index properties (e_{min}) have been formulated. A simplified procedure for the determination of a set of material constants using these correlations has been proposed.

In future, the empirical functions (e.g. f_p at large pressures, f_e at small void ratios) will be inspected to extend their range of applicability. Long-term tests are indispensable for an evaluation of the function f_N at larger numbers of cycles $N > 10^5$.

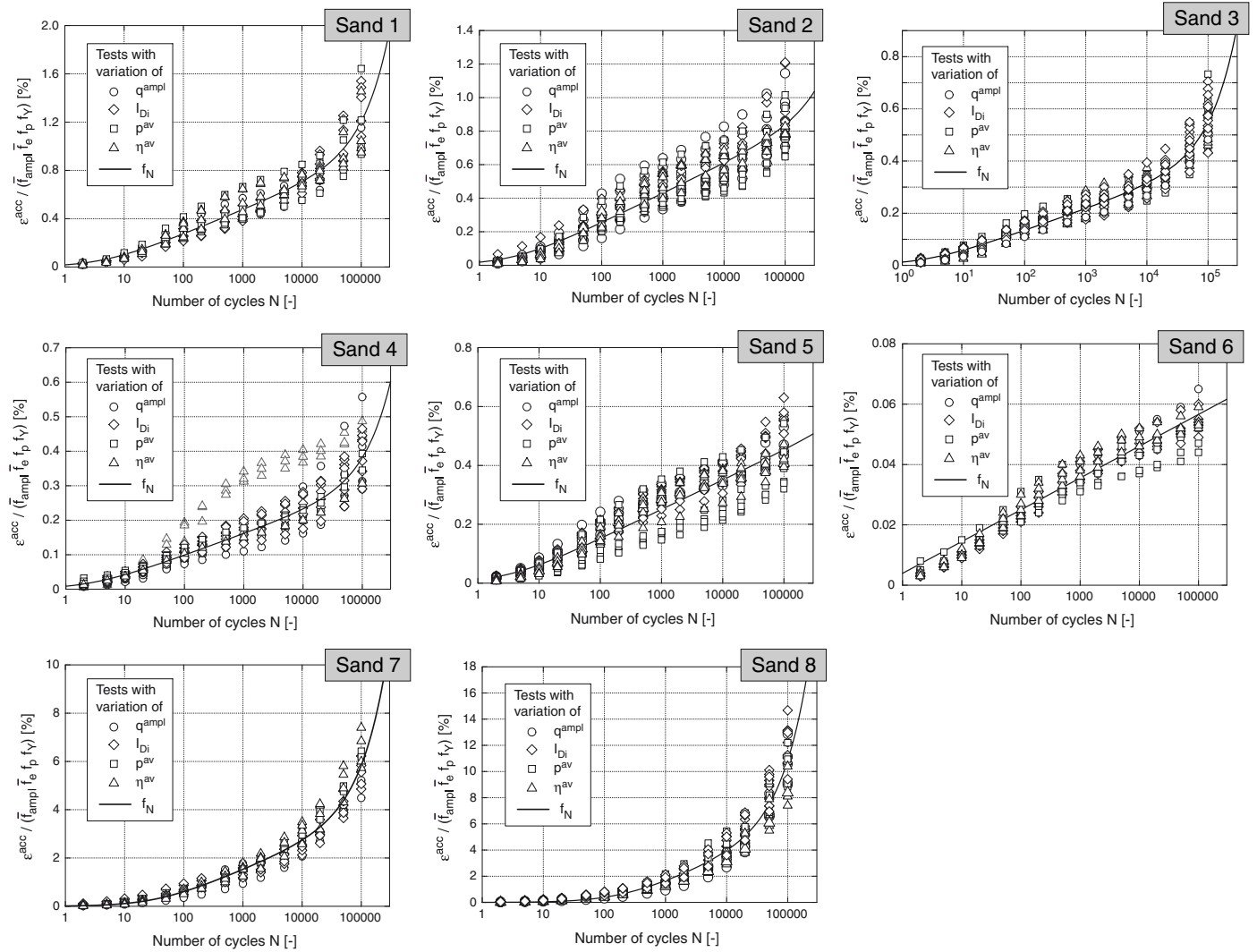


Fig. 21: Curves $\epsilon^{acc}(N)/(\bar{f}_{amp}\bar{f}_e\bar{f}_p\bar{f}_\gamma)$, fitting of function f_N

ACKNOWLEDGEMENT

The study presented in the paper has been performed in the framework of the project A8 "Influence of the fabric changes in soil on the lifetime of structures" of SFB 398 "Lifetime oriented design concepts" during the former work of the authors at Ruhr-University Bochum, Germany. The authors are grateful to DFG (German Research Council) for the financial support.

References

- [1] M. Abdelkrim, P. De Buhan, and G. Bonnet. A general method for calculating the traffic load-induced residual settlement of a platform, based on a structural analysis approach. *Soils and Foundations*, 46(4):401–414, 2006.
- [2] G. Bouckovalas, R.V. Whitman, and W.A. Marr. Permanent displacement of sand with cyclic loading. *Journal of Geotechnical Engineering, ASCE*, 110(11):1606–1623, 1984.
- [3] G. Castro and S.J. Poulos. Factors affecting liquefaction and cyclic mobility. *Journal of the Geotechnical Engineering Division, ASCE*, 103(GT6):501–516, 1977.
- [4] J.L. Chaboche. Constitutive equations for cyclic plasticity and cyclic viscoplasticity. *International Journal of Plasticity*, 5:247–302, 1989.
- [5] J.L. Chaboche. Modelling of ratchetting: evaluation of various approaches. *European Journal of Mechanics*, 13(4):501–518, 1994.
- [6] C.S. Chang and R.V. Whitman. Drained permanent deformation of sand due to cyclic loading. *Journal of Geotechnical Engineering, ASCE*, 114(10):1164–1180, 1988.
- [7] V.A. Diyaljee and G.P. Raymond. Repetitive load deformation of cohesionless soil. *Journal of the Geotechnical Engineering Division, ASCE*, 108(GT10):1215–1229, 1982.
- [8] P.M. Duku, J.P. Stewart, D.H. Whang, and E. Yee. Volumetric strains of clean sands subject to cyclic loads. *Journal of Geotechnical and Geoenvironmental Engineering, ASCE*, 134(8):1073–1085, 2008.
- [9] S. Goto, F. Tatsuoka, S. Shibuya, Y.-S. Kim, and T. Sato. A simple gauge for local small strain measurements in the laboratory. *Soils and Foundations*, 31(1):169–180, 1991.
- [10] A. Gotschol. Veränderlich elastisches und plastisches Verhalten nichtbindiger Böden und Schotter unter zyklisch-dynamischer Beanspruchung. Dissertation, Universität Gh Kassel, 2002.
- [11] S.J. Hain. An application of cyclic triaxial testing to field model test. In *International Symposium on Soils under cyclic and transient loading*, pages 23–31. Balkema, Rotterdam, Januar 1980. Swansea.

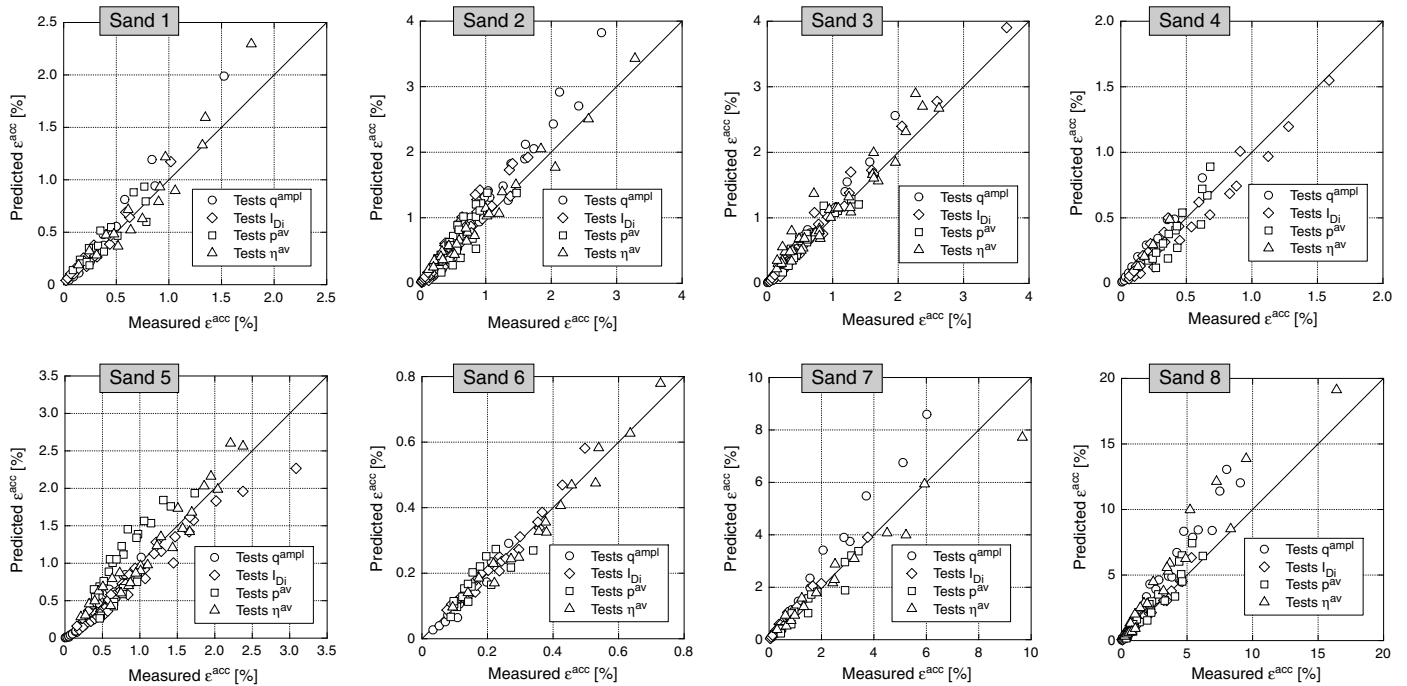


Fig. 22: Comparison of the residual strain ε^{acc} predicted by the HCA model with the constants given in Table 3 and the measured values from the cyclic triaxial tests. The data points correspond to $N = 10^2, 10^3, 10^4$ and 10^5 cycles, respectively.

- [12] E. Hoque, T. Sato, and F. Tatsuoaka. Performance evaluation of LDTs for use in triaxial tests. *Geotechnical Testing Journal, ASTM*, 20(2):149–167, 1997.
- [13] K. Ishihara. *Soil Behaviour in Earthquake Geotechnics*. Oxford Science Publications, 1995.
- [14] W.S. Kaggwa, J.R. Booker, and J.P. Carter. Residual strains in calcareous sand due to irregular cyclic loading. *Journal of Geotechnical Engineering, ASCE*, 117(2):201–218, 1991.
- [15] T. Kokusho, T. Hara, and R. Hiraoka. Undrained shear strength of granular soils with different particle gradations. *Journal of Geotechnical and Geoenvironmental Engineering, ASCE*, 130(6):621–629, 2004.
- [16] K.L. Lee and J.A. Fitton. Factors affecting the cyclic loading strength of soil. In *Vibration Effects of Earthquakes on Soils and Foundations, ASTM Special Technical Publication 450*, pages 71–95, 1969.
- [17] R.W. Lentz and G.Y. Baladi. Simplified procedure to characterize permanent strain in sand subjected to cyclic loading. In *International Symposium on soils under cyclic and transient loading*, pages 89–95. Balkema, Rotterdam, Januar 1980.
- [18] M.P. Luong. Mechanical aspects and thermal effects of cohesionless soils under cyclic and transient loading. In *Proc. IUTAM Conf. on Deformation and Failure of Granular materials, Delft*, pages 239–246, 1982.
- [19] W.A. Marr and J.T. Christian. Permanent displacements due to cyclic wave loading. *Journal of the Geotechnical Engineering Division, ASCE*, 107(GT8):1129–1149, 1981.
- [20] H. Matsuoka and T. Nakai. A new failure criterion for soils in three-dimensional stresses. In *Deformation and Failure of Granular Materials*, pages 253–263, 1982. Proc. IUTAM Symp. in Delft.
- [21] M. Miner. Cumulative damage in fatigue. *Transactions of the American Society of Mechanical Engineering*, 67:A159–A164, 1945.
- [22] Z. Mróz, V.A. Norris, and O.C. Zienkiewicz. An anisotropic hardening model for soils and its application to cyclic loading. *Int. J. Numer. Anal. Meth. Geomech.*, 2:203–221, 1978.
- [23] A. Niemunis. Extended hypoplastic models for soils. Habilitation, Veröffentlichungen des Institutes für Grundbau und Bodenmechanik, Ruhr-Universität Bochum, Heft Nr. 34, 2003. available from www.pg.gda.pl/~aniem/an-liter.html.
- [24] A. Niemunis and I. Herle. Hypoplastic model for cohesionless soils with elastic strain range. *Mechanics of Cohesive-Frictional Materials*, 2:279–299, 1997.
- [25] A. Niemunis, T. Wichtmann, and T. Triantafyllidis. A high-cycle accumulation model for sand. *Computers and Geotechnics*, 32(4):245–263, 2005.
- [26] A. Niemunis, T. Wichtmann, and Th. Triantafyllidis. On the definition of the fatigue loading for sand. In *International Workshop on Constitutive Modelling - Development, Implementation, Evaluation, and Application, 12-13 January 2007, Hong Kong*, 2007.
- [27] R. Pyke, H.B. Seed, and C.K. Chan. Settlement of sands under multidirectional shaking. *Journal of the Geotechnical Engineering Division, ASCE*, 101(GT4):379–398, 1975.
- [28] A. Sawicki and W. Świdziński. Compaction curve as one of basic characteristics of granular soils. In E. Flavigny and D. Cordary, editors, *4th Colloque Franco-Polonais de Mécanique des Sols Appliquée*, volume 1, pages 103–115, 1987. Grenoble.
- [29] A. Sawicki and W. Świdziński. Mechanics of a sandy subsoil subjected to cyclic loadings. *Int. J. Numer. Anal. Meth. Geomech.*, 13:511–529, 1989.
- [30] M.J. Shenton. Deformation of Railway Ballast under repeated loading conditions. *Railroad track mechanics and technology*. Pergamon Press, pages 405–425, 1978.
- [31] M.L. Silver and H.B. Seed. Deformation characteristics of sands under cyclic loading. *Journal of the Soil Mechanics and Foundations Division, ASCE*, 97(SM8):1081–1098, 1971.

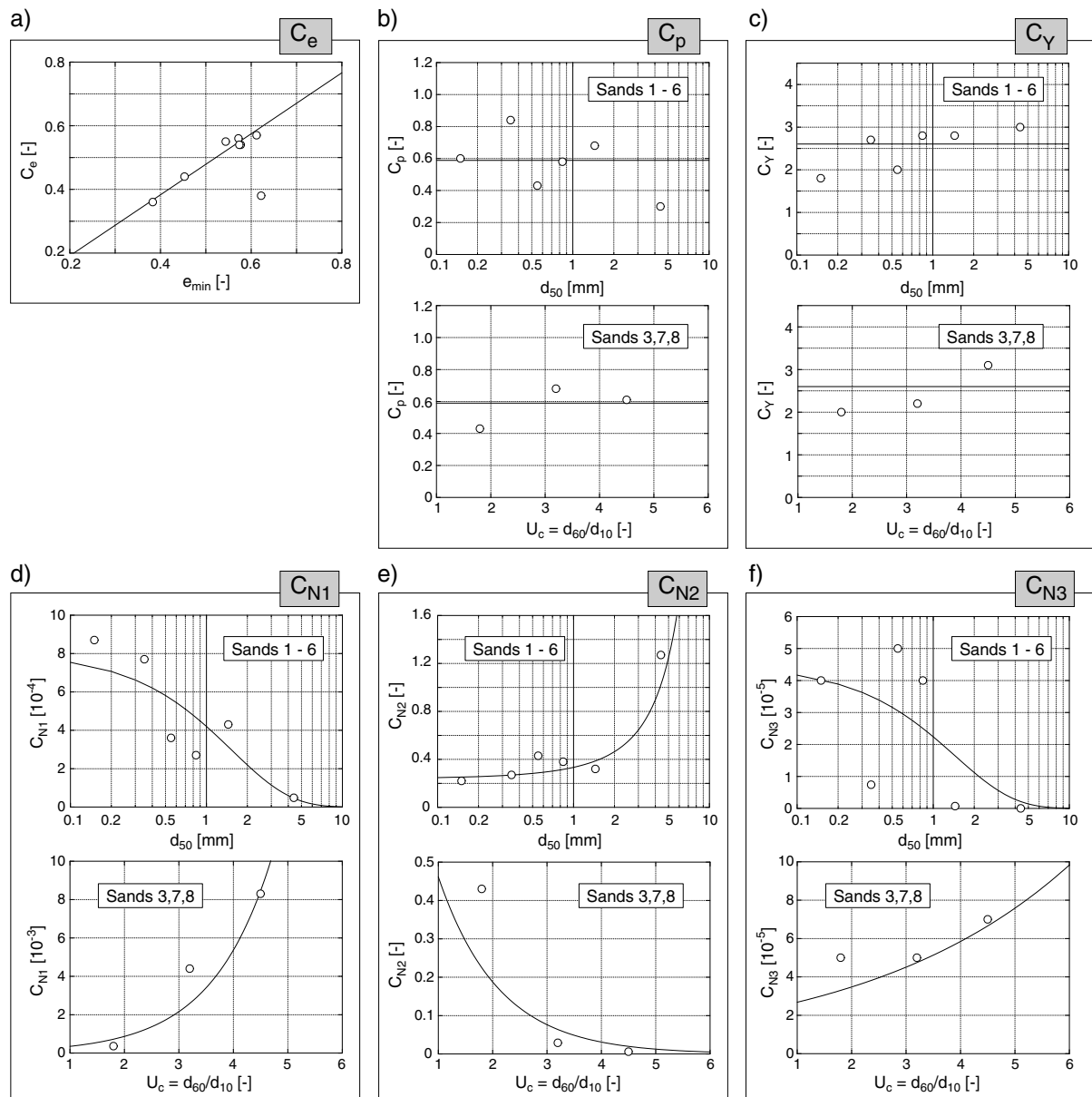


Fig. 23: Correlation of constant C_e with e_{\min} and correlations of constants C_p , C_Y , C_{N1} , C_{N2} and C_{N3} with d_{50} and U_c

- [32] M.L. Silver and H.B. Seed. Volume changes in sands during cyclic loading. *Journal of the Soil Mechanics and Foundations Division, ASCE*, 97(SM9):1171–1182, 1971.
- [33] A.S.J. Suiker, E.T. Selig, and R. Frenkel. Static and cyclic triaxial testing of ballast and subballast. *Journal of Geotechnical and Geoenvironmental Engineering, ASCE*, 131(6):771–782, 2005.
- [34] F. Tatsuoaka, S. Toki, S. Miura, Kato H., M. Okamoto, S.-I. Yamada, S. Yasuda, and F. Tanizawa. Some factors affecting cyclic undrained triaxial strength of sand. *Soils and Foundations*, 26(3):99–116, 1986.
- [35] I. Towhata. *Geotechnical Earthquake Engineering*. Springer, 2008.
- [36] Y. Tsukamoto, K. Ishihara, S. Sawada, and T. Kanno. Residual deformation characteristics of partially saturated sandy soils subjected to seismic excitation. In *Proc. 11th Int. Conf. on Soil Dynamics and Earthquake Engineering, Berkeley, Calif.*, volume 1, pages 694–701, 2004.
- [37] Y.P. Vaid, J.M. Fisher, R.H. Kuerbis, and D. Negussey. Particle gradation and liquefaction. *Journal of Geotechnical Engineering, ASCE*, 116(4):698–703, 1990.
- [38] K.C. Valanis and C.F. Lee. Endochronic theory of cyclic plasticity with applications. *Journal of Applied Mechanics*, 51:367–374, 1984.
- [39] P.-A. von Wolffersdorff. A hypoplastic relation for granular materials with a predefined limit state surface. *Mechanics of Cohesive-Frictional Materials*, 1:251–271, 1996.
- [40] T. Wichtmann. Explicit accumulation model for non-cohesive soils under cyclic loading. PhD thesis, Publications of the Institute of Soil Mechanics and Foundation Engineering, Ruhr-University Bochum, Issue No. 38, available from www.rz.uni-karlsruhe.de/~gn97/, 2005.
- [41] T. Wichtmann, A. Niemunis, and T. Triantafyllidis. Strain accumulation in sand due to cyclic loading: drained triaxial tests. *Soil Dynamics and Earthquake Engineering*, 25(12):967–979, 2005.

- [42] T. Wichtmann, A. Niemunis, and T. Triantafyllidis. On the influence of the polarization and the shape of the strain loop on strain accumulation in sand under high-cyclic loading. *Soil Dynamics and Earthquake Engineering*, 27(1):14–28, 2007.
- [43] T. Wichtmann, A. Niemunis, and T. Triantafyllidis. Strain accumulation in sand due to cyclic loading: drained cyclic tests with triaxial extension. *Soil Dynamics and Earthquake Engineering*, 27(1):42–48, 2007.
- [44] T. Wichtmann, A. Niemunis, and T. Triantafyllidis. On the determination of a set of material constants for a high-cycle accumulation model for non-cohesive soils (in print). *Int. J. Numer. Anal. Meth. Geomech.*, 34(4):409–440, 2010.
- [45] Y. Yamada and K. Ishihara. Yielding of loose sand in three-dimensional stress conditions. *Soils and Foundations*, 22(3):15–31, 1982.
- [46] S. Yasuda and M. Soga. Effects of frequency on undrained strength of sands (in Japanese). In *Proc. 19th Nat. Conf. Soil Mech. Found. Eng.*, pages 549–550, 1984.
- [47] Y. Yoshimi and H. Oh-Oka. Influence of degree of shear stress reversal on the liquefaction potential of saturated sand. *Soils and Foundations*, 15(3):27–40, 1975.
- [48] T.L. Youd. Compaction of sands by repeated shear straining. *Journal of the Soil Mechanics and Foundations Division, ASCE*, 98(SM7):709–725, 1972.